African Journal of Engineering Research and Innovation

AJERI Vol 4. No. 1. 2026

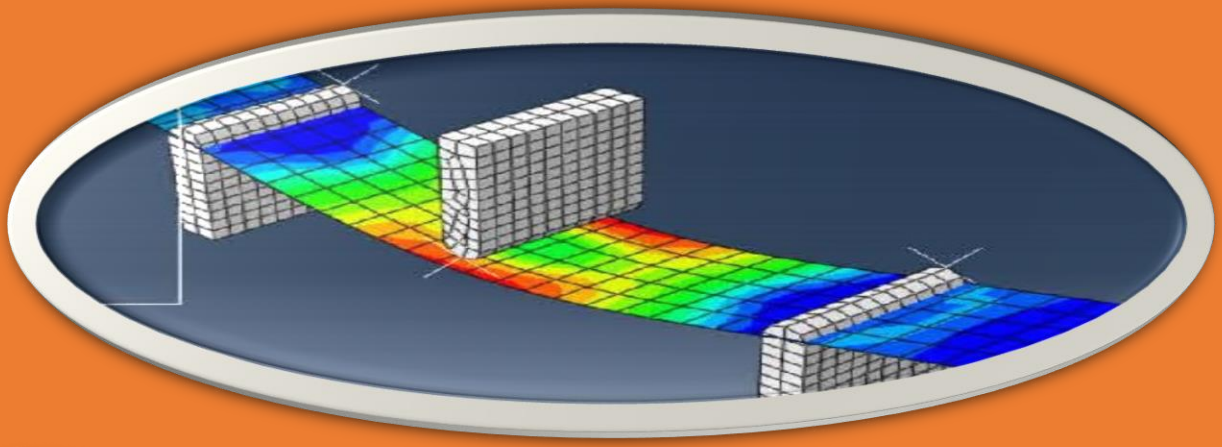

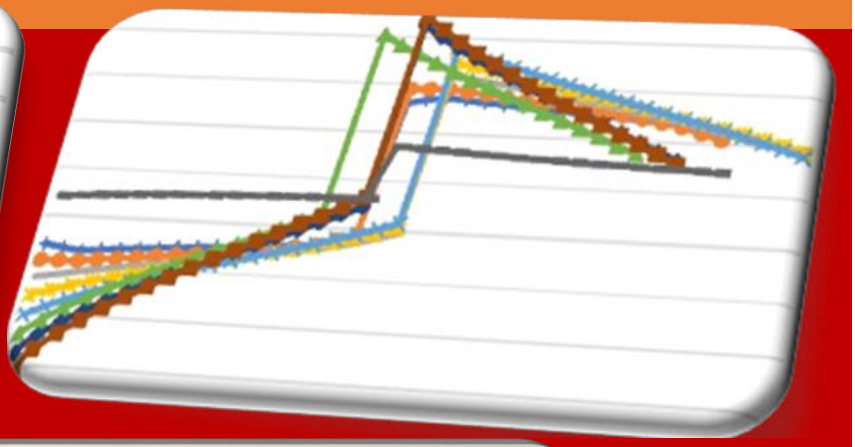

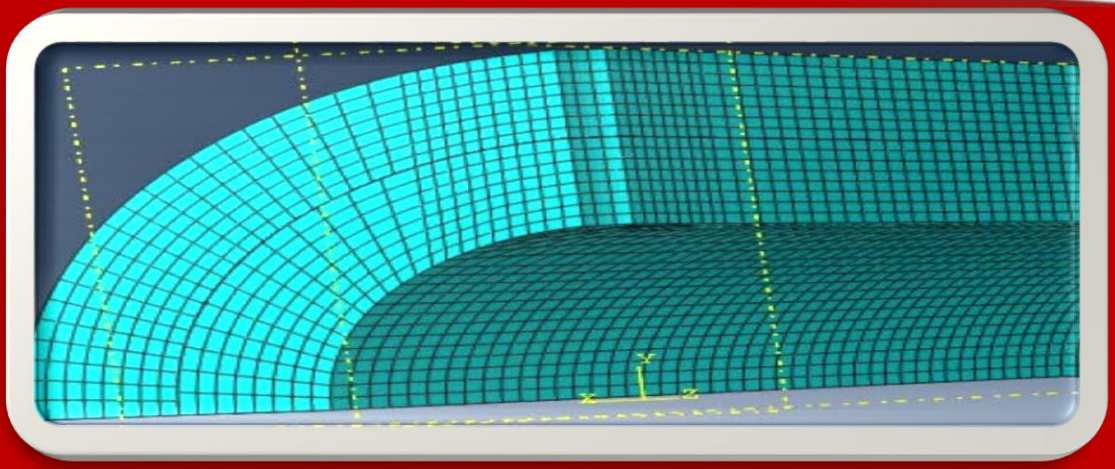

The Institution of Engineers of Kenya

ISSN: 2957- 7780

In partnership with

ISSN: 2957- 7780

AJERI

African Journal of Engineering in Research and Innovation

ISSN: 2957- 7780 Volume 4. No 1. 2026

IEK

Published by:

The *Institution of Engineers of Kenya*

P.O Box 41346- 00100

Nairobi Kenya

Tel: +254 (20) 2729326, 0721 729363, (020) 2716922

Email: editor@iekenya.org

Website: www.iekenya.org

African Journal of Engineering Research and Innovation (AJERI), is published by **The *Institution of Engineers of Kenya,*** IEK, as an international forum for publication of high-quality papers in all areas of Engineering

ISSN: 2957- 7780

CONTENTS **Pages**

Performance Evaluation of Septic Tanks in Kitale Town, Trans Nzoia County, Kenya

N. Maluki[*1], S. Kipchirchir[1], S. M. Njoroge[1]

[1] Department of Civil and Structural Engineering, Moi University, Eldoret, Kenya

[*]Corresponding Author: pureben1790@gmail.com

Abstract

Treatment of wastewater is crucial to protect human health and the ecosystem. Septic tanks physically and microbially treat wastewater. With rapid population growth and increasing wastewater from new apartments, septic tanks face potential overloading, risking contamination of surface and groundwater. The objective of this study was to evaluate the performance of septic tanks in Kitale town. The study methods involved field observations and laboratory analysis of influent and effluent samples from twenty septic tanks located in the study area. The findings revealed that 3 septic tanks (15%) experienced overloading and increased pollutant levels. Fourteen, (70%) septic tanks did not meet effluent discharge standards for key parameters such as Chemical Oxygen Demand (COD), Biochemical Oxygen Demand (BOD), and Total Suspended Solids (TSS). It was concluded that population density and usage patterns such as peak usage times and volume of wastewater discharged significantly influenced septic tank loading rates and performance efficiency. Maintenance practices, including desludging frequency, odour control measures, and the presence of additives and soak pits, played a crucial role in overall system efficiency. It was recommended that the Trans-Nzoia County Government should implement regular monitoring of loading conditions and consider upgrading to offsite sanitation in high-population areas. Further research should focus on innovative treatment technologies to enhance the efficiency of septic systems and improve pollutant removal.

Keywords: Septic tank, wastewater quality, treatment efficiency, quality parameters, discharge characteristics, Kitale, Kenya

1. Introduction

Wastewater management is a critical environmental and public health issue worldwide. Domestic wastewater contains various pollutants, including organic matter, pathogens, and chemical contaminants (Singh et al., 2022). Effective wastewater treatment is necessary to prevent contamination and protect public health (Capodaglio, 2017). In many developing countries, including Kenya, a significant portion of the population relies on on-site sanitation systems such as septic tanks (Kanoti, 2021). Septic tanks act as primary treatment units but often discharge effluent with high levels of nutrients, BOD, COD, and pathogens, which can threaten water resources if not properly managed (USEPA, 2008). Decentralized systems require regular maintenance to prevent overloading and failure (Rashid et al., 2021). In peri-urban areas like Kitale Town, population growth has raised concerns about the sustainability of existing septic systems, which are often poorly maintained and overloaded (Mumma et al., 2011).

Effluent from septic tanks can contaminate groundwater with nitrates, phosphates, and microbial pathogens such as E. coli (Peiyue-Li, 2021). Adegoke and Stenstrom (2019) emphasize the need for improved treatment technologies to enhance effluent quality. Solutions such as anaerobic biofilters and constructed wetlands have been proposed (El-Zanfaly et al., 2011). Despite their widespread use, data on the performance of septic tanks in peri-urban areas like Kitale are limited. This study addresses this gap by assessing septic tank loading, maintenance, and treatment efficiency in Kitale Town. Parameters such as BOD, COD, TSS, and microbial contaminants were analysed to determine compliance with Kenya's Water Quality Regulations (2006).

This study assessed septic tank loading, maintenance, treatment efficiency, and wastewater characteristics.

2. Materials and Methods

2.1 Study Area

Kitale town is located in Trans-Nzoia County, in the Rift Valley region of Kenya. It is the largest town in the county and serves as the administrative center and covers an area of approximately 146 km^2. Kitale is located at 1° 0′ 56" North, 35° 0′ 22" East, and at an elevation of around 1,897 m above mean sea level. It is 62 km from Eldoret, 326 km from Nairobi and 766 km from Mombasa. The population for Kitale was 162,174 in 2019 and is projected to rise to 216,301 by 2027 (KNBS, 2019, CIDP 2023-2027).

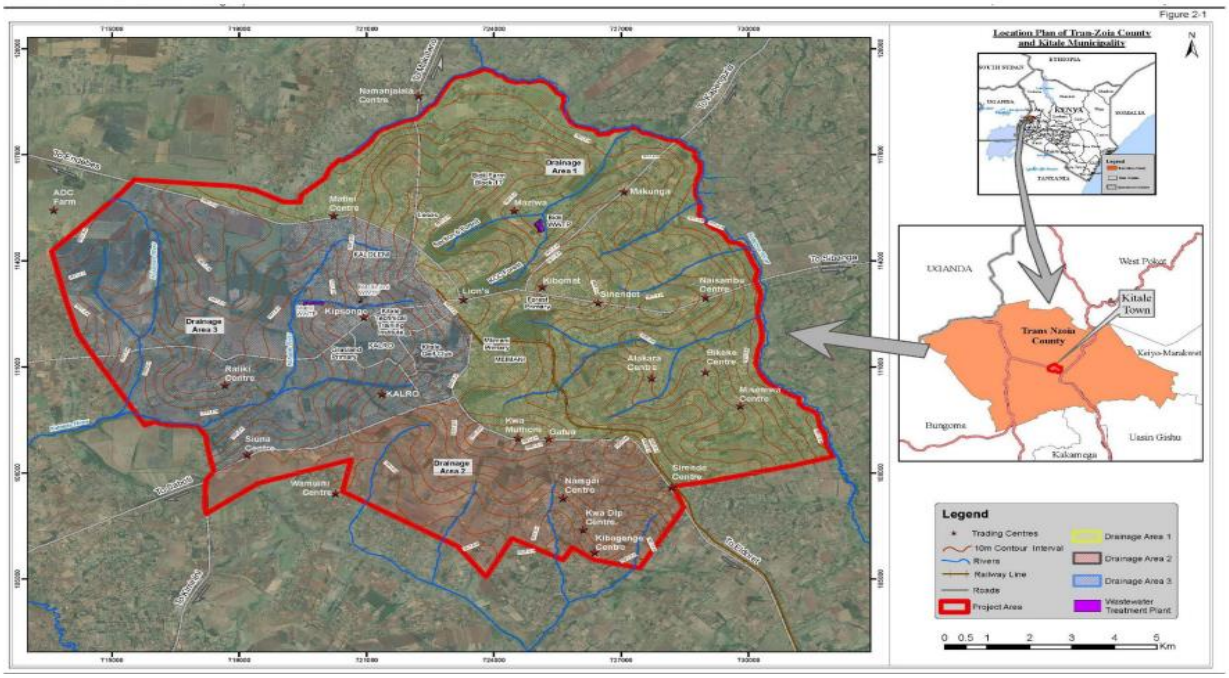

Figure 1: Kitale Municipality Map (Source: Kitale Municipality ISUDP)

2.2 Methodology

The study assessed septic tank loading, maintenance, treatment efficiency, and wastewater characteristics. The sample size was determined using Cochran's formula (Cochran, 1977), where a total of 20 septic tanks from residential (10), institutional (2), municipality (5), and industrial (3) areas were selected. Sampling points were identified using GIS data from Google Earth Pro as shown in figure 2 below.

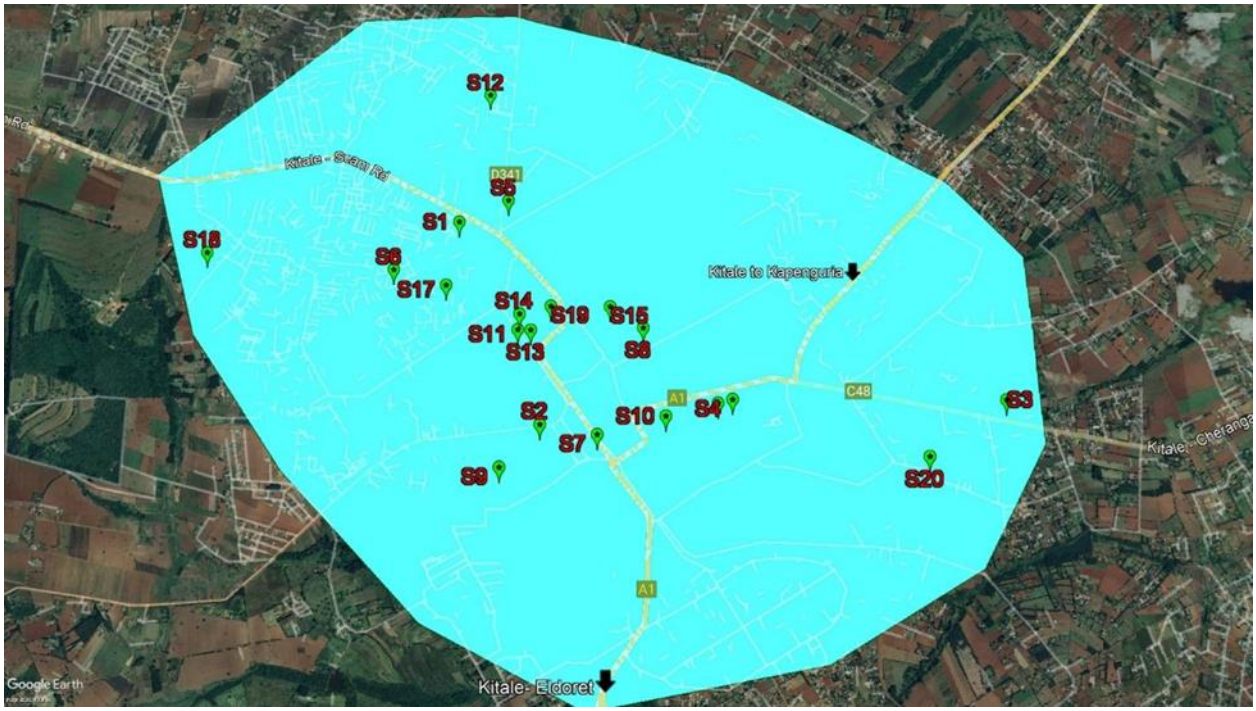

Figure 2: Sampling sites

2.2.1 Loading and Maintenance of Septic Tanks

Loading characteristics were evaluated by identifying greywater or blackwater sources, signs of overloading, leaks, and calculating hydraulic loading rate based on population and discharge volume. Hydraulic loading rate was calculated using the following relationship:

Hydraulic loading rate = Population* water consumption (in m^3 per day per person) *80%/Septic volume (in $m^{3)}$. This relationship assumed 80% of water used in a household became wastewater.

Maintenance practices were assessed by examining desludging frequency (within 3–5 years), tank accessibility, soak pit condition, odors, and use of additives.

2.2.2 Treatment Efficiency of Septic Tanks

Treatment efficiency was determined by analyzing physical parameters (temperature, total solids, oil and grease), chemical parameters (pH, COD, alkalinity), and biological parameters (BOD and E. coli). All these parameters' compliance was checked against the Kenya Water Regulations Act 2006 for maximum allowable effluent discharge to the environment. The wastewater temperature measurement was done in the field for each septic tank, using alcohol-in-glass thermometer while the Ph was measured using the Ph meter.

The total settleable solids were read from the graduations of the Imhoff cone after it was filled with the sample and allowed to settle for one hour. TSS was measured by filtering a well-mixed sample through a standard glass fibre filter and drying the residue retained on the filter at 103 to 105 degrees (Oyaya, 2021). The filter's weight increase represents the amount of total suspended solids. Total dissolved solids were read using the EC/TDS meter.

The oil and grease were extracted from the samples by intimate contact with petroleum ether and noting the weight difference between a conical flask with residue after evaporation and one without residue.

Other wastewater characteristics (BOD, COD, alkalinity and Ph) were determined using standard methods summarised here. BOD tests measure was done over five days to determine BOD_5 (Lee, 2012) while COD was measured by the closed reflux method (LaPara et al., 2000). The alkalinity was determined using the photometer method where, the alkaphot M tablet was used (Banchamlak, 2021). The membrane filtration technique was used to test for presence of E-Coli.

3. Results and Discussion

3.1 Loading Characteristics of septic tanks

Table 1 below gives the observed septic tanks' loading characteristics.

Table 1: Septic tanks' loading characteristics

	Site	Type of raw water	Population size (persons)	Septic size (m^3)	Hydraulic Loading Rate ($m^3/m^2/day$))	Leaks at the top	Overloading
RH	S1	Combined	120	45	0.64	Yes	Yes
School	S2	Combined	1520	60	2.0267	No	No
RH	S3	Combined	156	48	0.26	No	No
School	S4	Combined	827	60	1.1027	No	No
RH	S5	Combined	106	45	0.1884	No	No
RH	S6	Separate	150	45	0.2667	No	No
MCP	S7	Combined	70	30	0.1867	No	No
IAT	S8	Combined	84	45	0.1493	No	No
IAT	S9	Combined	94	45	0.1671	No	No
RH	S10	Combined	103	60	0.1373	No	No
MCP	S11	Combined	56	48	0.0933	No	No
RH	S12	Combined	132	60	0.176	Yes	Yes
MCP	S13	Combined	80	60	0.1067	No	No
MCP	S14	Combined	68	60	0.0907	No	No
RH	S15	Combined	12	24	0.04	No	No
RH	S16	Combined	7	24	0.0233	Yes	Yes
RH	S17	Combined	20	40	0.04	No	No
RH	S18	Combined	27	48	0.045	No	No
MCP	S19	Combined	90	54	0.1333	No	No
IAT	S20	Combined	30	42	0.0571	No	No

When the volume or rate of wastewater entering the septic tank exceeds its designed capacity, the detention time may be reduced (Vivaraghavan, 1976). This reduction in detention time can lead to several observable problems like overloaded drain field, high amounts of solids in the effluent, foul odours, slow draining fixtures, visible signs of effluent around the tank and increased pumping frequency. Only sites 1, 12 and 16 were overloaded. Physical observations common in these sites were the leaks at the top in S1 and S16 and overflow in the soak pit of

S12. Sites with high population and small size of tank like S1 were overloaded, evidenced by leaks at the top of the septic tank.

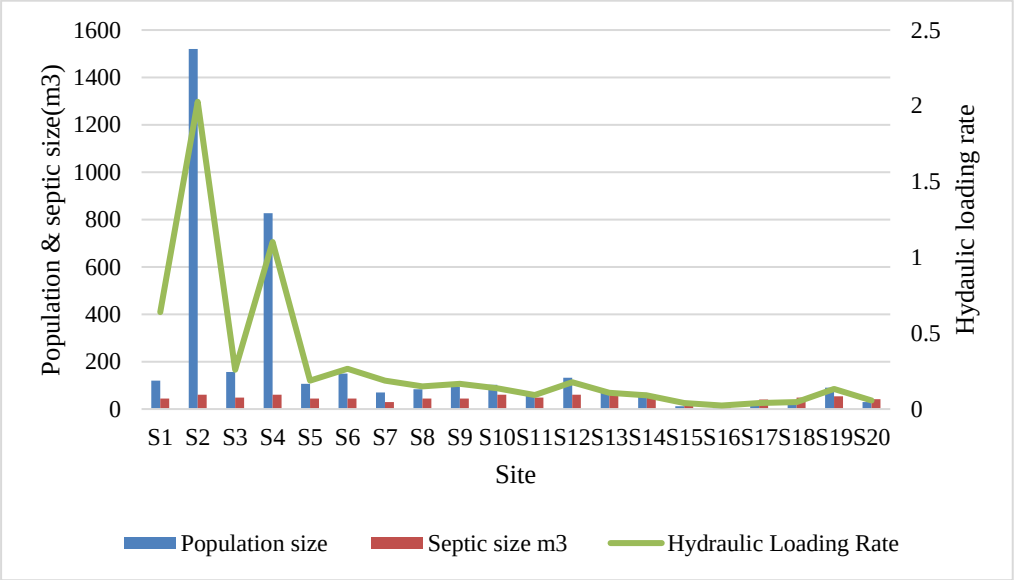

Figure 3: Population and Hydraulic loading rates

The graph above shows that hydraulic loading rate is affected by population and septic tank size; a higher population with a small size of tank results in a higher hydraulic loading rate. These results are in agreement with research conducted by Abbassi et al. (2018) that showed that hydraulic loading rates are affected by population size and the size of the septic size.

3.2 Maintenance characteristics of septic tanks

Table 2 below gives the maintenance of septic tanks.

Table 1: Septic tanks' maintenance checklist

Site Location	**desludging frequency (years)**	**Odour (0-1)**	**presence of additives**	**presence of soak pits**
S1	6	1	Yes	No
S2	3	0	Yes	Yes
S3	5	1	Yes	No
S4	3	1	No	Yes
S5	3	0	Yes	Not visible
S6	5	0	Yes	No
S7	3	1	Yes	Yes
S8	4	1	Yes	No
S9	3	1	Yes	Yes

Site Location	desludging frequency (years)	Odour (0-1)	presence of additives	presence of soak pits
S10	2	1	No	No
S11	5	1	Yes	No
S12	5	1	Yes	Yes
S13	5	1	Yes	No
S14	5	0	No	Yes
S15	5	1	Yes	No
S16	6	0	Yes	No
S17	5	0	Yes	No
S18	5	1	No	No
S19	5	1	Yes	Yes
S20	5	1	No	Yes

Desludging is typically done every 4 years to prevent solids buildup (Leong et al., 2022). Site S10 had a 2-year frequency indicating heavier water use, while S1 and S16 had 6-year intervals. Odor levels were generally lower with more frequent desludging, though this was not always consistent (Boon & Vincent, 2003). Additives like hydrogen peroxide and alum, as used in S19, can improve performance but also increase odours if overused (El-Zanfaly et al., 2011). Soak pits were present at 40% of sites and improved performance, while S2 and S14 used advanced soak trenches.

3.3 Treatment Efficiency of Septic Tanks

3.3.1 Physical parameters

Tabel 3 shows results from the laboratory tests carried out on septic tanks wastewater influent and effluent to determine their physical characteristics.

Table 2: Septic tank influent and effluent physical characteristics

Site Description	Site No.	TDS (mg/l)			TSS			Temperature		OIL & GREASE (mg/l)		
		Influent	Effluent	Efficiency %	Influent	Effluent	Efficiency %	Influent	Effluent	Influent	Effluent	Efficiency %
RH	S1	315.6	456.5	-44.6	247.0	85.3	65.5	21.6	21.6	21.0	5.0	76.2
SCH	S2	365.9	187.0	48.9	476.5	234.0	50.9	20.7	20.7	42.0	6.0	85.7
RH	S3	415.5	312.0	24.9	314.0	78.9	74.9	20.7	20.7	26.0	7.0	73.1
SCH	S4	382.0	115.0	69.9	120.0	98.0	18.3	19.5	20.7	27.0	9.0	66.7
RH	S5	268.9	98.0	63.6	147.0	115.0	21.8	19.0	20.7	15.0	10.0	33.3
RH	S6	218.0	45.0	79.4	300.0	42.0	86.0	19.0	19.5	27.0	5.0	81.5
MCP	S7	755.0	205.0	72.8	105.0	35.0	66.7	19.0	20.7	34.0	6.0	82.4
IAT	S8	312.0	214.0	31.4	178.0	150.0	15.7	20.1	20.0	26.0	4.0	84.6
IAT	S9	238.9	115.7	51.6	324.0	170.0	47.5	20.7	20.0	26.0	7.0	73.1
RH	S10	526.9	278.3	47.2	100.0	90.0	10.0	20.1	20.8	15.0	2.0	86.7
MCP	S11	497.4	287.3	42.2	108.0	93.4	13.5	19.2	20.9	32.0	2.0	93.8
RH	S12	364.6	233.7	35.9	123.0	35.0	71.5	19.2	19.0	29.0	6.0	79.3
MCP	S13	650.0	220.0	66.2	108.0	18.0	83.3	20.9	23.0	18.0	7.0	61.1
MCP	S14	608.0	312.0	48.7	378.0	57.0	84.9	21.0	21.0	29.0	10.0	65.5
RH	S15	418.0	125.0	70.1	127.0	37.0	70.9	21.0	20.0	12.0	8.0	33.3
RH	S16	650.0	340.0	47.7	213.0	65.4	69.3	20.0	19.9	29.0	12.0	58.6
RH	S17	455.0	193.6	57.5	238.0	98.0	58.8	20.7	21.0	36.0	7.0	80.6
RH	S18	315.0	107.3	65.9	312.0	111.5	64.3	19.8	19.0	28.0	3.0	89.3
MCP	S19	276.5	117.9	57.4	435.0	125.0	71.3	21.4	20.0	31.0	4.0	87.1
IAT	S20	209.5	67.7	67.7	125.0	27.0	78.4	20.3	20.7	17.0	9.0	47.1

Oil and grease

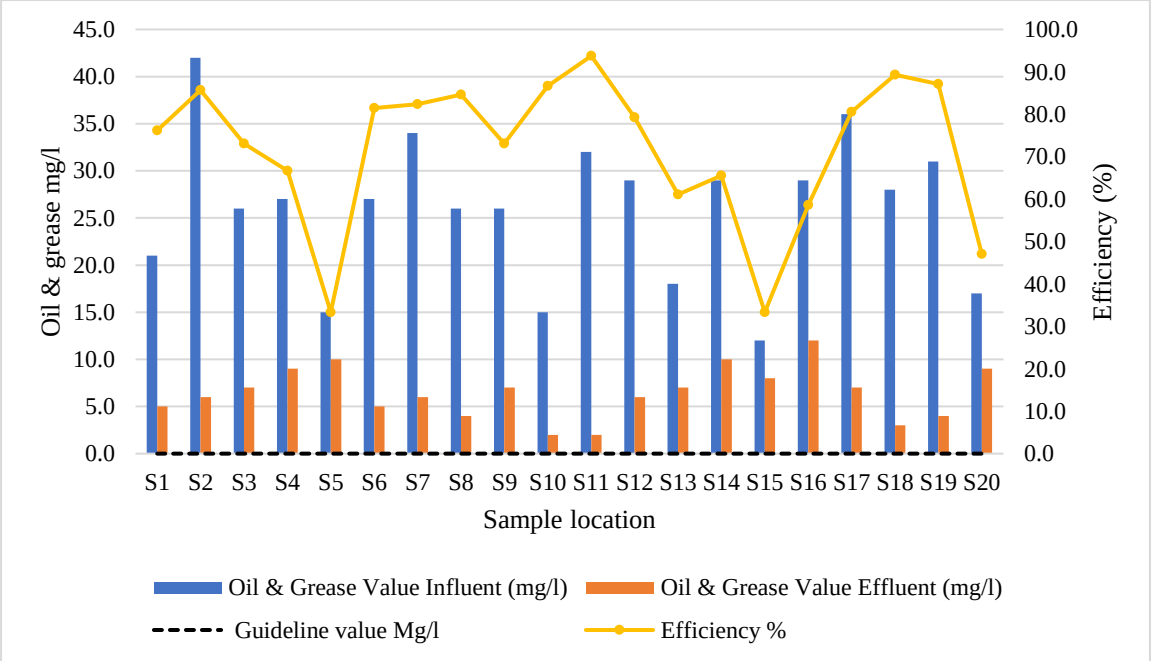

Figure 4: Oil and Grease removal efficiency

All septic tank effluents exceeded the allowable oil and grease limit of 0 mg/l (Water Quality Regulations, 2006), with Site S16 recording the highest level at 12.0 mg/l and Sites S10 and S11 the lowest at 2.0 mg/l. Removal efficiency ranged from 33.3% at S5 to 93.8% at S11, where high scum levels contributed to better oil and grease conversion.

Total Suspended Solids (TSS)

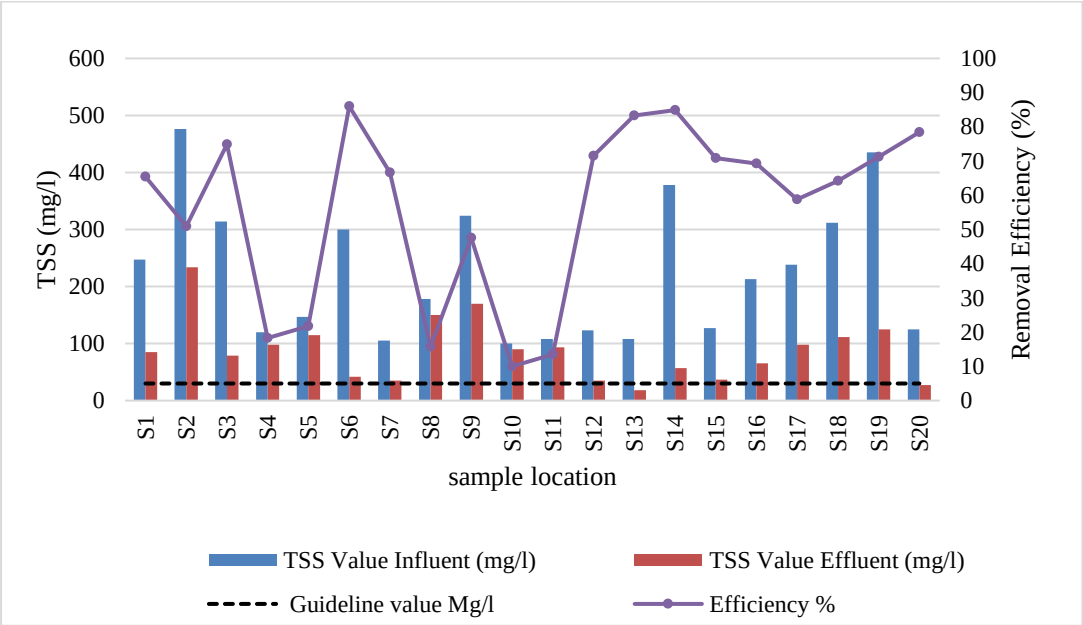

Figure 5: TSS Removal efficiency

Total suspended solids (TSS) exceeded the allowable limit of 30 mg/l (Water Quality Regulations, 2006) at all sites except S13 (mg/L), with S2 recording the highest level at 234 mg/l due to a high population. S6 achieved the highest removal efficiency at 86.0%.

Total Dissolved Solids (TDS)

TDS values ranged from 45 mg/l (S6) to 456.47 mg/l (S1), with S1 (mg/L) showing elevated effluent levels due to overloading and infrequent desludging. All sites met removal efficiency standards ((Water Quality Regulations, 2006)) except S1.

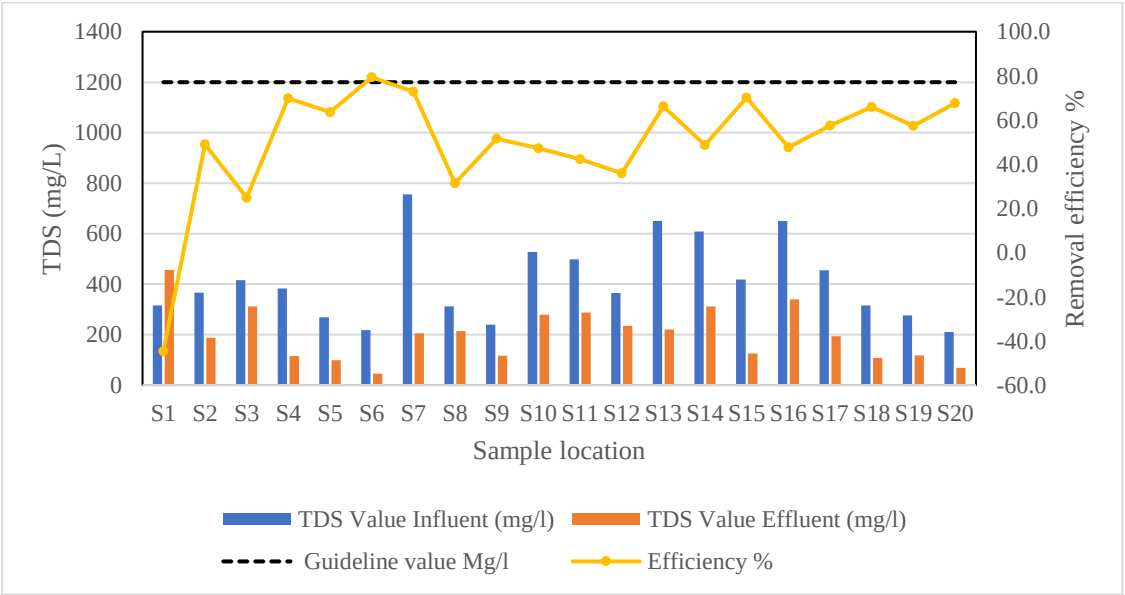

Figure 6: TDS removal efficiency

Temperature

The temperature of the septic effluent was measured on site and it ranged from 19 to 21.6°C. The effluent temperature was slightly lower than the ambient temperature which was about 25 °C because all the septic tanks were installed underground.

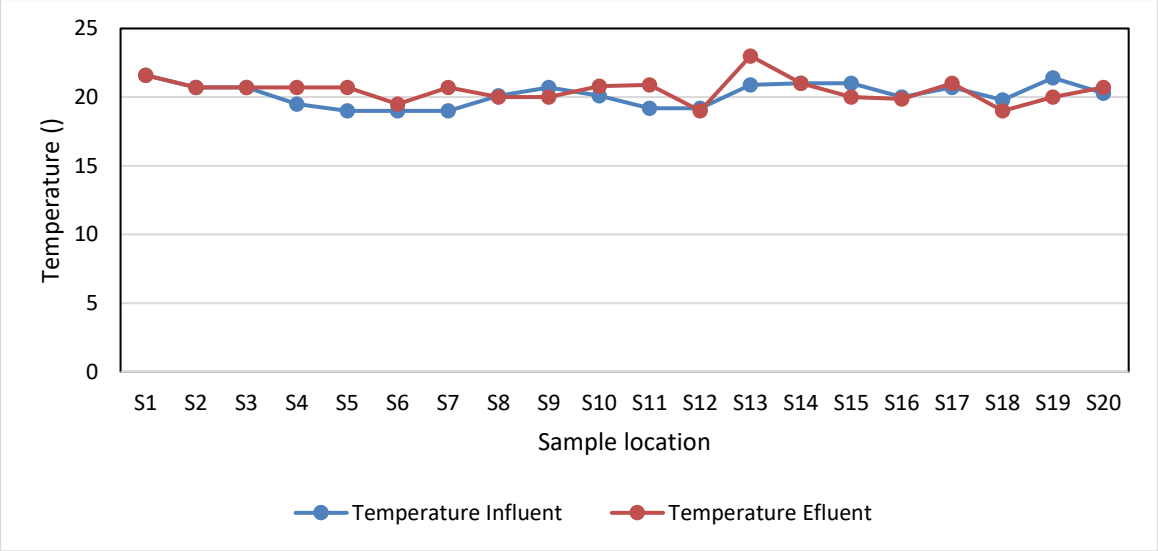

Figure 7: Influent and Effluent Temperatures

3.3.2 Chemical characteristics

Table 4 shows the results from the laboratory tests carried out on septic tanks wastewater influent and effluent to determine their chemical characteristics.

Table 3: Septic tank effluent chemical characteristics

		Ph		Alkalinity			COD		
Site Description	Site No.	Influent	Effluent	Influent	Effluent	Efficiency	Influent	Effluent	Efficiency %
RH	S1	5.5	5.8	205.0	210.0	-2.4	556.8	499.2	10.3
SCH	S2	5.8	6.5	243.0	265.0	-9.1	585.6	250.7	57.2
RH	S3	5.8	6.0	180.0	205.0	-13.9	835.0	196.0	76.5
SCH	S4	6.8	7.2	800.0	837.0	-4.6	633.0	406.0	35.9
RH	S5	6.3	6.7	210.0	304.0	-44.8	485.8	307.2	36.8
RH	S6	6.7	7.0	680.0	1000.0	-47.1	633.0	434.1	31.4
MCP	S7	5.8	6.6	312.0	486.0	-55.8	897.5	529.9	41.0
IAT	S8	6.6	6.7	920.0	980.0	-6.5	794.9	588.8	25.9
IAT	S9	5.8	6.6	455.0	600.0	-31.9	989.6	647.7	34.5
RH	S10	5.5	6.0	210.0	300.0	-42.9	397.4	278.9	29.8
MCP	S11	6.4	7.0	289.0	435.0	-50.5	559.4	395.4	29.3
RH	S12	6.8	7.2	375.0	516.0	-37.6	485.8	603.5	-24.2
MCP	S13	5.8	7.5	196.0	365.0	-86.2	610.0	255.0	58.2
MCP	S14	6.5	6.9	587.0	642.0	-9.4	805.5	299.3	62.8
RH	S15	6.6	7.3	790.0	881.0	-11.5	1055.7	413.0	60.9
RH	S16	6.9	7.3	903.0	944.0	-4.5	548.7	301.0	45.1
RH	S17	6.0	7.4	857.0	1110.0	-29.5	554.0	192.0	65.3
RH	S18	6.7	7.6	789.0	840.0	-6.5	1005.5	380.8	62.1
MCP	S19	6.7	7.0	690.0	700.0	-1.4	897.9	488.9	45.6
IAT	S20	6.8	7.8	788.0	976.0	-23.9	678.9	224.0	67.0

Chemical Oxygen Demand (COD)

The COD values ranged from 192 mg/l from S17 to 647.7mg/l in S9. All the COD values were above the guideline value of 50 mg/l (Water Quality Regulations, 2006). The efficiencies recorded were low compared to removal efficiency of other parameters. The highest efficiency was 67% from S20 and the lowest 24.2% from S12. Site S12 reported overloading with low treatment efficiency. The high COD value of 603.52mg/l explains the high level of odour from that site (Hu, 2005).

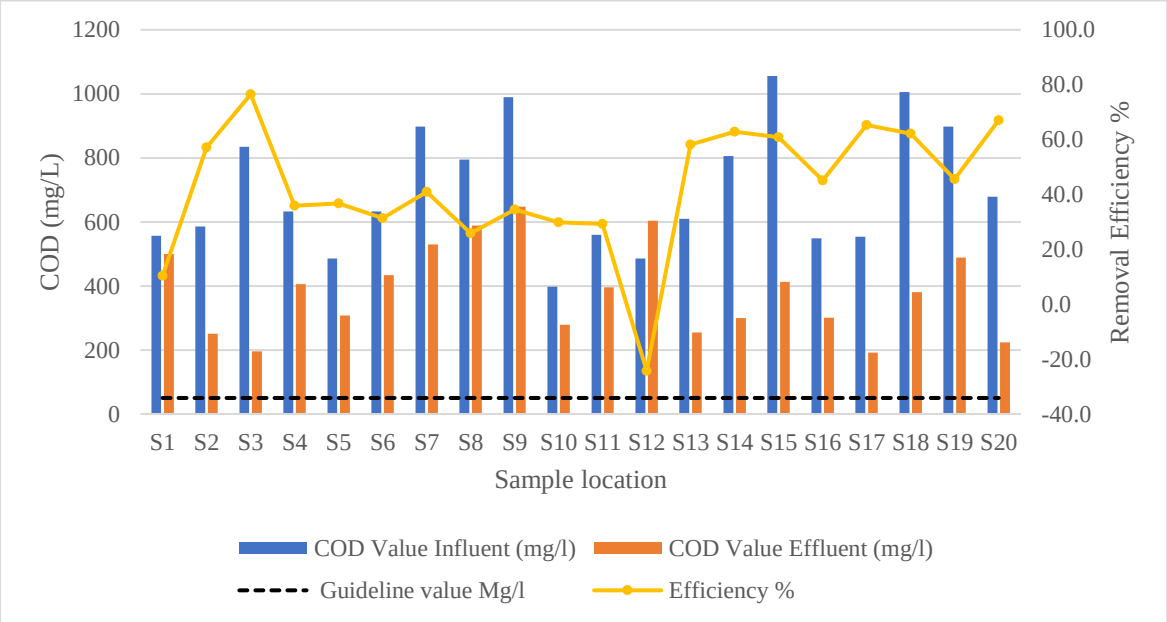

Figure 8: COD treatment efficiency

Alkalinity

Total alkalinity ranged from 205 mg/l (S3) to 1110 mg/l (S17), with low alkalinity values correlating with low pH levels, such as in S1 (210 mg/l, pH 5.8). All sites exceeded the 150 mg/l guideline value set by the (Water Quality Regulations, 2006). The lowest removal efficiency was -86.2% in S13, while S19 showed the highest at -1.4%, with negative efficiency due to higher alkalinity in effluent than influent. Elevated alkalinity levels may stem from mineral-rich groundwater sources commonly used in the area (Rosborg, & Kozisek, 2016)).

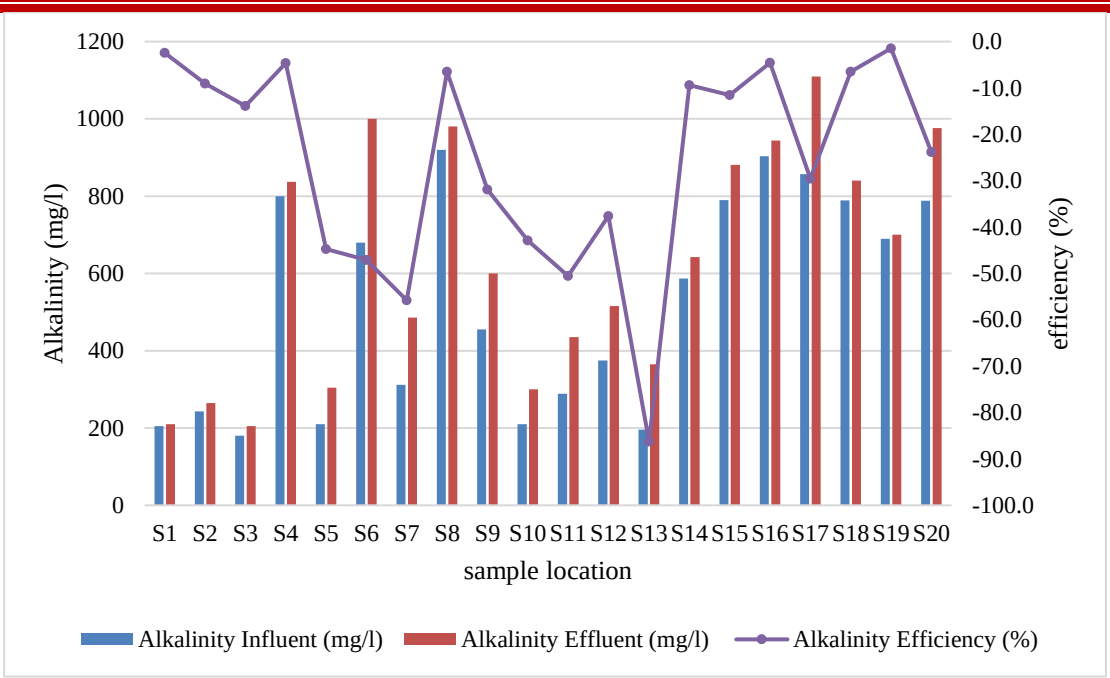

Figure 9: Alkalinity treatment efficiency

pH

The pH values for the effluent ranged from 5.8 in S1 to 7.8 in S20, with low pH in S1 linked to overloading, chemical additives, and low alkalinity (210 mg/l), contributing to high odor (Kasima, 2014. While 17 sites met the effluent guideline range of 6.5–8.5, sites S1, S3, and S10 did not (Water Quality Regulations, 2006).

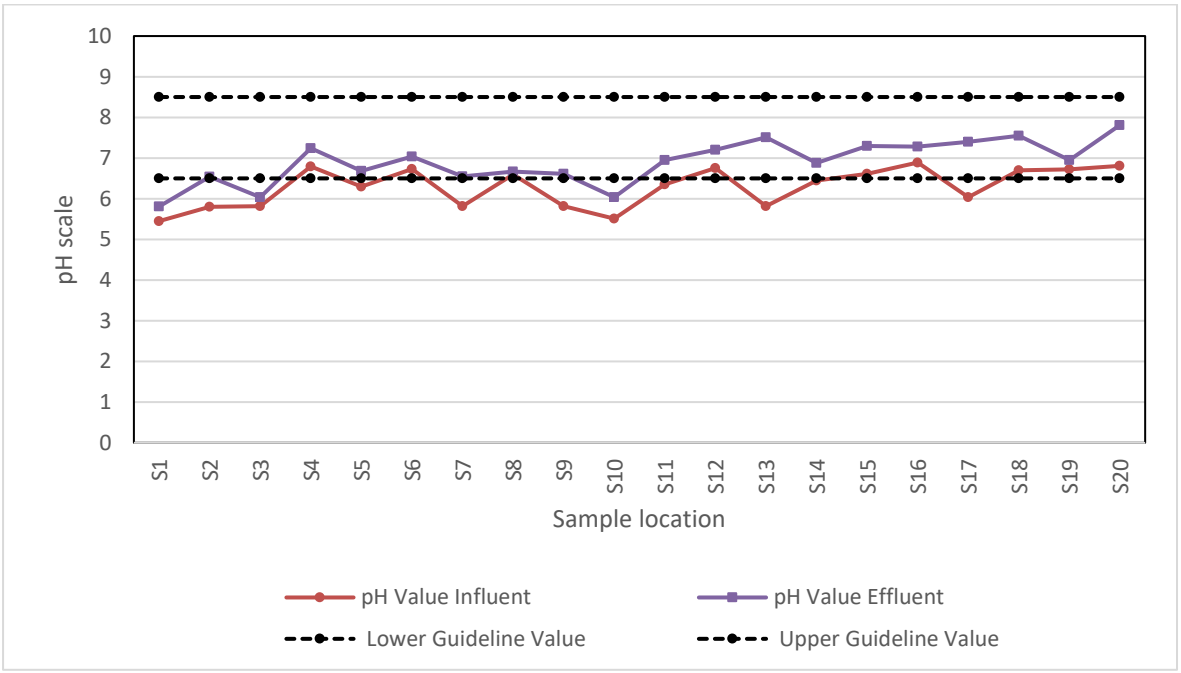

Figure 10: Wastewater influent and effluent pH values

3.3.3 Biological characteristics

Table 5 gives the results from the laboratory tests carried out on the samples to determine their biological characteristics.

Table 4: Biological Characteristics of Septic Tanks Wastewater influent and effluent

Site Description	Site No.	E.COLI (CFU/100ml) Influent	Effluent	Efficiency %	BOD (mg/L) Influent	Effluent	Efficiency %
RH	S1	84.0	10.0	88.1	110.0	98.0	10.9
SCH	S2	56.0	12.0	78.6	250.0	125.0	50.0
RH	S3	45.0	20.0	55.6	118.0	77.0	34.7
SCH	S4	89.0	18.0	79.8	150.0	30.0	80.0
RH	S5	67.0	8.0	88.1	108.0	28.0	74.1
RH	S6	98.0	15.0	84.7	140.0	65.0	53.6
MCP	S7	53.0	14.0	73.6	215.0	127.0	40.9
IAT	S8	86.0	11.0	87.2	180.0	68.0	62.2
IAT	S9	77.0	17.0	77.9	150.0	78.0	48.0
RH	S10	55.0	7.0	87.3	170.0	101.0	40.6
MCP	S11	64.0	13.0	79.7	128.5	67.0	47.9
RH	S12	45.0	9.0	80.0	87.0	43.0	50.6
MCP	S13	96.0	22.0	77.1	127.5	48.6	61.9
MCP	S14	85.0	12.0	85.9	101.0	58.4	42.2
RH	S15	72.0	16.0	77.8	75.6	43.2	42.9
RH	S16	34.0	18.0	47.1	110.0	45.4	58.7
RH	S17	94.0	14.0	85.1	198.0	88.0	55.6
RH	S18	54.0	15.0	72.2	117.5	42.3	64.0
MCP	S19	67.0	11.0	83.6	98.0	37.7	61.5
IAT	S20	90.0	13.0	85.6	89.0	23.0	74.2

E-coli

Sites S1 and S5 had the highest faecal removal efficiency of 88.1% while S16 had the lowest removal efficiency of 47.1%. However, none of the 20 sites met the effluent discharge guideline of 0 cfu/100ml (Water Quality Regulations, 2006).

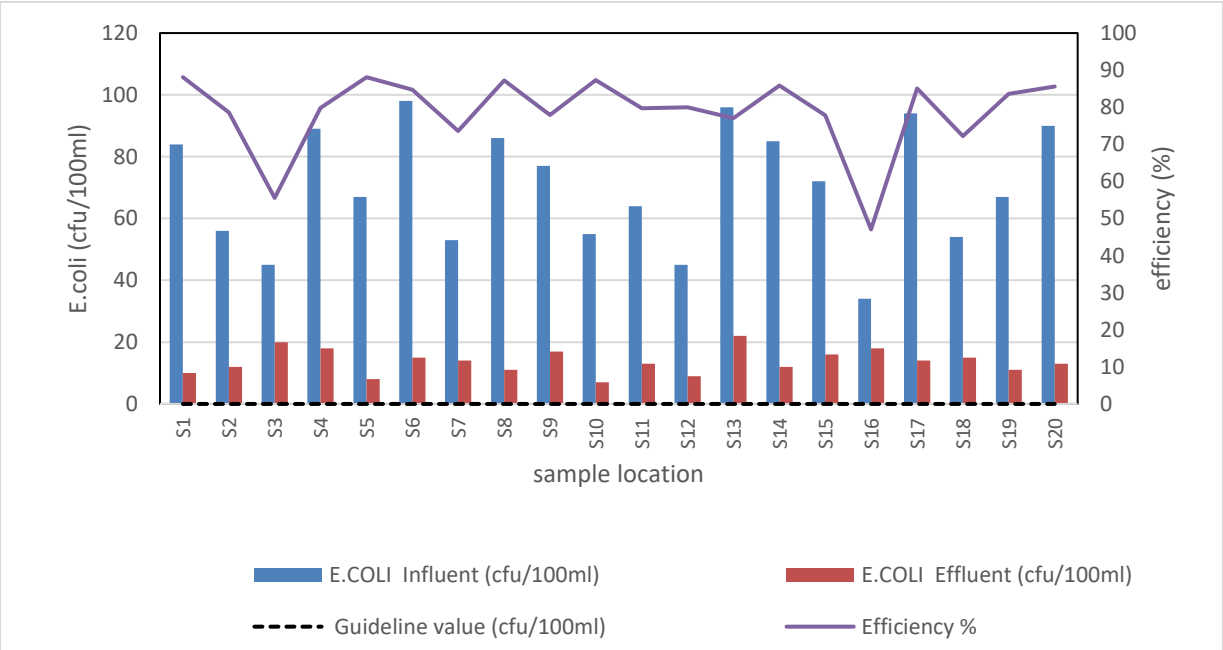

Figure 11: E-coli Treatment Efficiency

Biochemical Oxygen Demand (BOD)

BOD values ranged from 23 mg/l to 127 mg/l, with the highest level at Site 7 due to high TDS and the lowest at Site 20 linked to low TDS. Only Sites 4, 5, and 20 met the effluent guideline of 30 mg/l (Water Quality Regulations, 2006), with S4 showing the highest removal efficiency (80%) and S1 the lowest (10.9%). High BOD levels in S1 were associated with low pH and overloading (D. Lee, 2012).

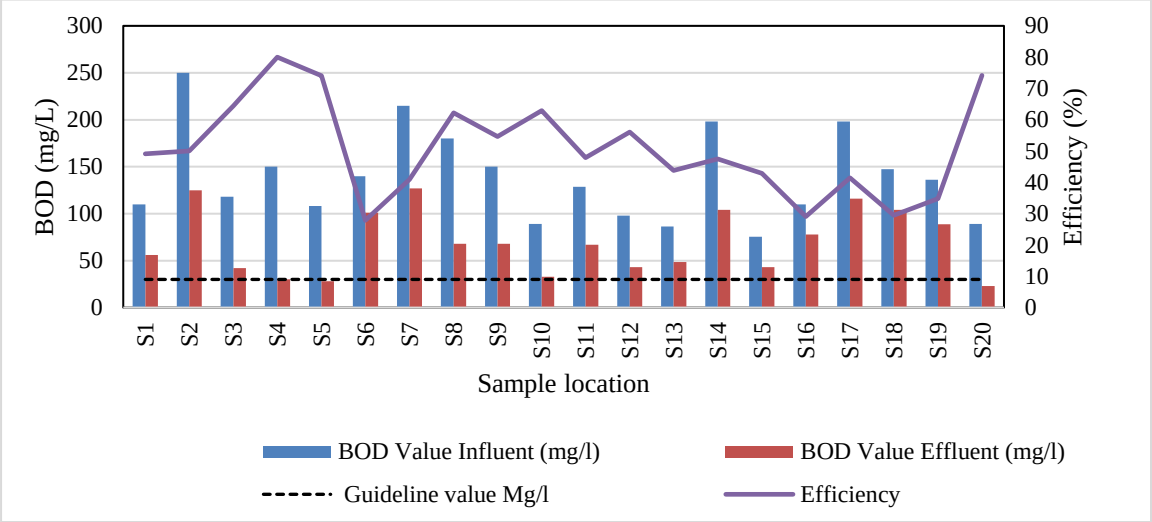

Figure 12: BOD Treatment Efficiency

4. Conclusion

4.1 Loading Conditions of septic tanks

The assessment of loading conditions revealed varying hydraulic loading rates among septic tanks in Kitale Town. Higher population sizes and small septic tank sizes were associated with increased loading rates, potentially leading to overloading and reduced treatment efficiency in some sites. This highlights the importance of considering population density when designing and managing septic systems.

4.2 Maintenance practices of septic tanks

The investigation into maintenance practices uncovered differences in desludging frequencies, odour control measures, and the presence of additives and soak pits among septic tank sites. Proper maintenance, including regular desludging and odour management, emerged as critical factors influencing treatment efficiency and overall system performance.

4.3 Treatment efficiency of septic tanks

The treatment efficiencies varied for all the parameters assessed (COD, BOD, E-coli, TDS, TSS and Oil & grease) in all the septic tanks studied. While some sites met effluent discharge standards, others exhibited elevated levels of pollutants such as COD, BOD, and E. coli, indicating suboptimal treatment performance. Factors such as overloading, inadequate maintenance, and influent characteristics contributed to these disparities.

Recommendations

1. To enhance septic system management, the Trans-Nzoia County Government should implement regular monitoring of loading conditions, conduct capacity assessments, consider upgrading to offsite sanitation in high-population areas, and enforce international standards for onsite effluent disposal systems.
2. Further research should focus on investigating innovative treatment technologies to improve the efficiency of septic systems and enhance pollutant removal.

References

Abbassi, B. E., Abuharb, R., Ammary, B., Almanaseer, N., & Kinsley, C. (2018). Modified septic tank: innovative onsite wastewater treatment system. Water, 10(5), 578.

Adegoke, A., & Stenstrom, T. A. (2019). Cesspits and Soakpits. Global Water Pathogen Project. Michigan State University, E. Lansing, MI, UNESCO. https://doi.org/10.14321/waterpathogens, 58.

Banchamlak, A. (2021). *Characterization and Treatment of Lake Tana Water for Drinking Purpose in Fogera Woreda* (Doctoral dissertation).

Capodaglio, Andrea G., and Gustaf Olsson. Energy issues in sustainable urban wastewater management: Use, demand reduction and recovery in the urban water cycle. Sustainability 12.1 (2019): 266.

D. Lee, B. (2012). Importance of Wastewater Biological Oxygen Demand in Septic Systems. p. 4.

Dalu, T., Banda, T., Mutshekwa, T., Munyai, L. F., & Cuthbert, R. N. (2021). Effects of urbanization and a wastewater treatment plant on microplastic densities along a subtropical river system. Environmental Science and Pollution Research, 28, 36102-36111.

Emeka, C., Nweke, B., Ihunwo, C. K., & Nta, S. (2021). Assessment of Groundwater Quality in Close Proximity to Septic Tanks and Potential Impact on Health. European Journal of Environment and Earth Sciences, 2(1), 8-10.

EPA. (2021). The Environmental Protection Agency Domestic Waste Water Treatment Systems (Population Equivalent ≤10).

Kanoti, J. R. (2021). *The Geometry, Hydro-geochemistry and Vulnerability of Aquifers to Pollution in Urban and Rural Settings-a Case Study of Kisumu and Mt. Elgon Aquifers* (Doctoral dissertation, University of Nairobi).

Kasima, E. (2014). Efficiency of municipal waste water treatment plants in Kenya: A case study of Mombasa Kipevu Treatment Works (Doctoral dissertation, University of Nairobi).

LaPara, T. M., Alleman, J. E., & Pope, P. G. (2000). Miniaturized closed reflux, colorimetric method for the determination of chemical oxygen demand. *Waste management*, *20*(4), 295-298.

Leong, W. K., Ngo, A. L. K., Wong, A. C. H., Ling, J. H., & Teck, H. (2022, May). The mandatory 4 years desludging frequency of underground septic tanks in residential areas: A case study in Sibu Sarawak, East Malaysia. In Journal of the Civil Engineering Forum (Vol. 8, No. 2).

Lukhabi, D. K., Mensah, P. K., Asare, N. K., Pulumuka-Kamanga, T., & Ouma, K. O. (2023). Adapted water quality indices: limitations and potential for water quality monitoring in Africa. Water, 15(9), 1736.

Mahlie, W. S. (1940). Oil and grease in sewage. Sewage Works Journal, 527-556.

MS, M. (2006). Potential for beneficial application of sulfate-reducing bacteria in sulfate-containing domestic wastewater treatment. Retrieved from link.springer.com: https://link.springer.com/article/10.1007/s11274-015-1935-x#:~:text=Sulfate%20is%20commonly%20present%20in,toilet%20flushing%20(Chen%20et%20al.pH and Water. (2019, October 22). Retrieved from usgs.gov.

Oyaya, C. (2021). A reflection on the development and implications of the Kenya environmental sanitation and hygiene policy 2016-2030. Academia Letters. https://doi.org/10.20935/al2861

Rashid, R., Shafiq, I., Akhter, P., Iqbal, M. J., & Hussain, M. (2021). A state-of-the-art review on wastewater treatment techniques: the effectiveness of adsorption method. Environmental Science and Pollution Research, 28, 9050-9066.

Rosborg, I., & Kozisek, F. (2016). Drinking water minerals and mineral balance. Springer International Pu, 1(1), 175.

Samie, A. (2017). Escherichia coli Recent Advances on Physiology, Pathogenesis and Biotechnical Applications. Bod Third Party Titles.

Singh, Nirankar, et al. "Challenges of water contamination in urban areas." Current directions in water scarcity research. Vol. 6. Elsevier, 2022. 173-202.

Slompo, N. D. M., Quartaroli, L., Fernandes, T. V., da Silva, G. H. R., & Daniel, L. A. (2020). Nutrient and pathogen removal from anaerobically treated black water by microalgae. Journal of Environmental Management, 268, 110693.

Smith, J. K., Johnson, L. R., & Brown, D. L. (2018). Effects of oil and grease on wastewater treatment. Journal of Environmental Engineering, 144(8), 04018059.

Talbott, J. (2021). Septic Tank Maintenance. Oregon State University Extension Service.

Viraraghavan, T. (1976). Septic tank efficiency. Journal of the Environmental Engineering Division, 102(2), 505-508.

Water Quality Regulations. (2006). Retrieved from https://www.nema.go.ke/images/Docs/water/water_quality_regulations.pdf

Z. Hu, D. G. (2005). Encyclopedia of Analytical Science (Second Edition)

Impulsive Noise Detection and Suppression in Power Line Communications (PLC) Using ANN

E. O. Odipo[1*], S. O. Awino[2], M. N. Ahuna[1]

[1]Department of Electrical and Electronics Engineering, the Technical University Kenya.

[2]Department of Physics, Pwani University.

*Corresponding author: Elly.Odipo@tukenya.ac.ke

Abstract

Power line communication (PLC) systems in the in- door low-voltage environments are heavily affected by impulsive noise generated by electrical switching events and transient disturbances. These noise events are random, high in amplitude, and not properly represented by conventional Gaussian assumptions, rendering reliable detection and mitigation particularly difficult. This paper presents an artificial neural network (ANN)–based approach for the detection and suppression of impulsive noise in PLC networks using measured noise data. The proposed frame- work exploits the short-term temporal dependence of impulsive noise by training a feedforward ANN to predict imminent noise samples from current observations. A decision-based suppression mechanism is then applied, where predicted noise spikes over a defined threshold are selectively suppressed. Experimental evaluation using real measurement data demonstrates that the proposed approach is effective in identifying impulsive noise events and reduces their impact besides preserving the integrity of the useful signal. The results confirm that ANN-driven prediction gives a data-adaptive and flexible solution for improving the robustness of PLC systems in impulsive noise–dominated networks.

Keywords —Power Line Communication (PLC), Low-voltage Networks, Impulsive Noise.

1. Introduction

Power line communication (PLC) has emerged as an attractive solution for data transmission in environments where dedicated communication infrastructure is either impractical or cost-prohibitive. By reusing existing electrical wiring, PLC enables connectivity for smart homes, energy monitoring, and automation systems without additional cabling [1], [2]. However, the same power delivery network that enables PLC also introduces a highly disturbed electromagnetic environment, particularly in indoor low-voltage installations where electrical loads are frequently switched and dynamically varied [1]–[4].

One of the dominant factors limiting the reliability of PLC systems is impulsive noise. Unlike background noise, which can often be approximated as stationary and Gaussian, impulsive noise manifests as sporadic, high-energy disturbances with short duration and random occurrence [1]–[4]. These impulses are normally generated by switching power supplies, motor drives, and protection devices connected to the electrical network [1]–[4]. Their unpredictable nature results in severe degradation of communication performance, more sore in terms of bit error rate and link stability. Previous work in [2] among others on PLC noise characterization confirmed that impulsive noise cannot be adequately described through the conventional additive white Gaussian noise models. Middleton's statistical approach generated one of the first systematic approaches to defining impulsive noise, showing its bursty and heavy-tailed characteristics [5], [6]. Subsequent measurement-based investigations in [7]–[9] further revealed that the indoor PLC noise possessed strong variability in time and amplitude excursions that rendered linear mitigation techniques difficult. To mitigate against these impairments, a range of impulsive noise suppression and mitigation frameworks have been explored. Traditional frameworks that include blanking, clipping, and linear filtering are computationally efficient [10], [11]. However, they depend on fixed thresholds or assumptions that fail adapt appropriately to the changing noise characteristics. In addition, these frameworks very often result in signal distortion or performance loss when noise characteristics vary rapidly. Recent works in [12] and [13] among others has introduced statistically driven methods that include adaptive thresholding and extreme value–based models that have resulted into improved robustness by accounting for the probabilistic characteristics of the rare but severe noise impulses. Currently, machine learning techniques have gained attention for their effective and efficient capabilities to learn complex nonlinear relationships like PLC noise directly from data. Specifically Artificial neural networks (ANNs), have demonstrated effectiveness in pattern recognition, time-series prediction, and nonlinear system modelling. Their use in addressing the PLC noise modelling problem, is

motivated by the observation that impulsive noise, although random, normally exhibits short-term temporal dependence that can be learned from measured data. The recent use of ANN-based noise classification and detection has produced promising results in the identification of impulsive events without explicit parametric noise models. Despite these advances, the use of ANN-based prediction for proactive impulsive noise suppression in PLC systems remains relatively least explored, specifically the use real indoor measurement data. The focus of several existing approaches is on post-detection mitigation and depend on simulated noise environments that often fail to fully capture the practical network conditions. This work seeks to address this gap by proposing an ANN-driven approach that predicts imminent impulsive noise samples from current observations and combines the prediction into a decision-based suppression mechanism. By integrating data-driven learning with selective suppression, the proposed model's objective is to enhance PLC robustness while preserving the integrity of the useful signal. The rest of the paper is organized as follows: In Section II, an analytical framework for ANN-based impulsive noise in the frequency range of 1−30 MHz is developed. Impulsive noise detection and suppression mechanism is discussed in Section III. Thereafter, impulsive noise acquisition and processing is presented in Section IV. In Section V, the results of the study is presented and finally the paper ends with concluding remarks in Section VI. II.

2. Analytical Framework for Ann-Based Impulsive Noise

A. Impulsive Noise Model for PLC with ANN-Based Input–Output Representation

The impulsive noise in PLC networks is non-Gaussian, time-varying, and characterized by high-amplitude, short duration impulses that dominate system performance if not properly mitigated [1], [2]. Let the received PLC signal be modelled as,

$$r(n) = s(n) + \varepsilon(n) + n_{imp}(n) \qquad (1)$$

where, s(n) is the transmitted data signal, ε(n) represents background Gaussian noise, and nimp(n) denotes impulsive noise, then accurate modelling of nimp(n) is crucial for effective and efficient detection and suppression. This motivates data-driven prediction techniques such as Artificial Neural Networks (ANN) to exploit the temporal structure present in the measured PLC noise [4], [5]. If the acquired PLC noise sample is arranged into an input vector through delay;

$$z(n) = [n_{imp}, n_{imp}(n-1), ..., n_{imp}(n-\zeta+1)]T \qquad (2)$$

with ζ defining the embedding dimension, then ANN learns the nonlinear mapping

$$\hat{n}_{imp}(n+1) = f(z(n); \vartheta) \qquad (3)$$

Where, nˆimp(n + 1) is the predicted impulsive noise, f(·) denotes the ANN function, and ϑ describes the network parameters that include the weights and biases.

B. Feedforward ANN Model

To augment the received PLC signal model in (1), a feedforward ANN is employed to learn the nonlinear temporal relationship present in impulsive PLC noise. The ANN maps a vector of previous noise samples to a future noise estimate, allowing short-term impulsive noise events prediction. As such, for a single hidden-layer feedforward network the ANN output is defined by [14], [15],

$$\hat{n}_{imp}(n+1) = \sum_{j=1}^{H} \omega_j^{(2)} \varphi\left(\sum_{k=1}^{\zeta} \omega_{jk}^{(1)} z_k(n) + b_j^{(1)} \right) + b^{(2)} \tag{4}$$

where, H is the number of hidden neurons, ω (1) jk and ω (2) j are input-to-hidden and hidden-to-output weights, b (1) j and b (2) are the biases, and φ(·) defines the activation function. By learning the temporal structure of acquired PLC noise, the ANN generates a data-driven prediction of future impulsive noise disturbances, which can be exploited for adaptive detection and suppression of in PLC systems.

C. Learning Criterion

The learning criterion used for the proposed ANN model by minimizing the prediction error between the measured impulsive noise sample nimp(n + 1) and its estimate nˆimp(n + 1).

The training objective is defined using the mean square error (MSE) criterion [14]–[16], using backpropagation with gradient descent with N defining the number of training samples.

$$\Psi = \frac{1}{N} \sum_{n=1}^{N} \left(n_{imp}(n+1) - \hat{n}_{imp}(n+1) \right)^2 \tag{5}$$

The weights are then updated based on [14]–[16],

$$\varrho^{(t+1)} = \varrho^{(t)} - \gamma \nabla_{\varrho} \Psi \tag{6}$$

where, γ is the learning rate. By minimizing Ψ, the proposed ANN model captures the temporal structure of the impulsive noise necessary for reliable and effective noise detection and suppression.

3. Impulsive Noise Detection and Suppression

The predicted impulsive noise, nˆimp(n) is compared with a predefined threshold λ [2], [17], [18], Impulsive noise event if

$$\hat{n}_{imp}(n) > \lambda \quad (7)$$

first to detect if an impulsive event is present. Once an impulse noise event is detected, suppression is effected through nonlinear filtering

$$\hat{r}(n) = \begin{cases} r(n) - \hat{n}_{imp}(n), & \text{if } \hat{n}_{imp}(n) > \lambda, \\ r(n), & \text{otherwise.} \end{cases} \quad (8)$$

Otherwise, the received signal is left unchanged. Such a decision-based operation allows for selective suppression of high-amplitude impulsive noise while preserving the useful signal in the non-impulsive noise intervals, hence improving the robustness of the PLC system in noisy environments.

4. Impulsive Noise Acquisition and Processing

Impulsive noise was acquired from a controlled machines laboratory environment within the university, representative of an indoor low-voltage power line network. The measurement setup as shown in Fig. 1 consisted of a high-resolution Rigol DS2202A digital storage oscilloscope (DSO) connected to standard mains outlet supplying typical laboratory electrical equipment, including rotating machines and power electronic drives, which naturally introduce switching transients and intermittent disturbances onto the power line as confirmed in [1], [3], [7], [9], [19]. A coupling interface was used to safely extract the high-frequency noise component from the power line without disrupting normal operation.

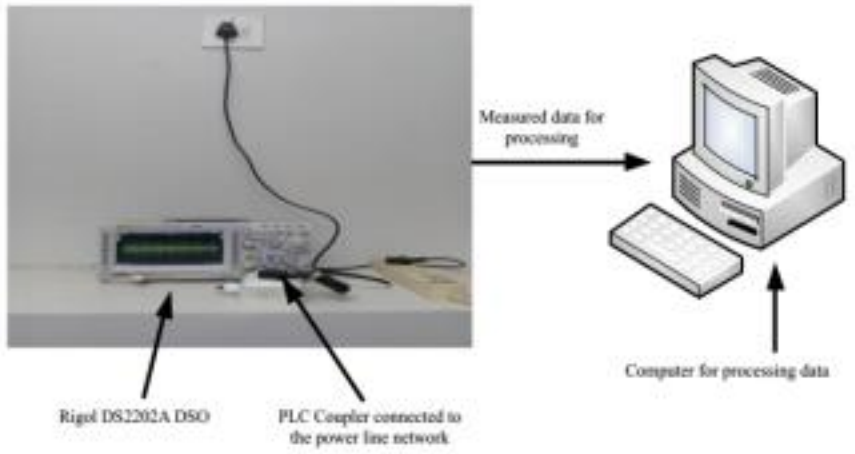

Fig. 1: Experimental set-up for PLC noise measurements [3].

This DSO was operated at a sampling rate of 2 Gigasamples per second, yielding a window length of 28 ms and was sufficient to resolve short-duration impulsive events. The recorded data were then transferred to a computer for offline processing. The resulting noise waveform shows sporadic high-amplitude impulses contained on a lower-level background, reflecting the bursty and time-localized nature of impulsive noise event in real low-voltage indoor PLC environments. A representative sample shown in Fig. 2 of the measured noise illustrates these abrupt excursions, which motivate the need for predictive and adaptive suppression techniques.

5. Results and Discussion

A. Model Training Results

In this training an ANN architecture of 3: 20: 1:1 as shown in Fig. 3 was realized.

This realized ANN architecture depicts a compact and sufficiently expressive network design based on the characteristics of the measured impulsive PLC noise.

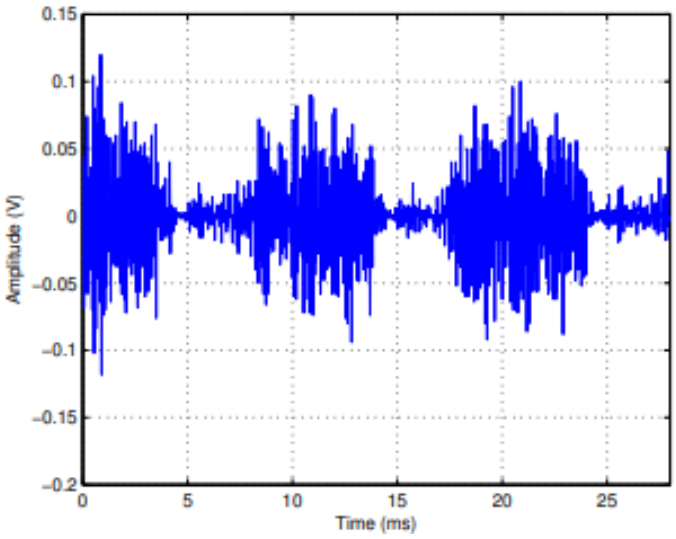

Fig. 2: Sample acquired impulsive noise

The historical noise samples are captured by the three input neurons and enables the network to capture short-term temporal behaviours present in the PLC noise. To provide a nonlinear modelling capability of handling the complex and random characteristics of impulsive noise, a single hidden layer comprising twenty neurons is included thus reducing excessive computational overhead. A single scalar estimate of the model output is generated at the single output neuron, while the final stage represents the regression output used for performance evaluation and subsequent suppression decisions. This developed architecture achieves a balance between prediction accuracy, training stability, and model simplicity, thus rendering it suitable for real-time or near–real-time PLC noise mitigation applications.

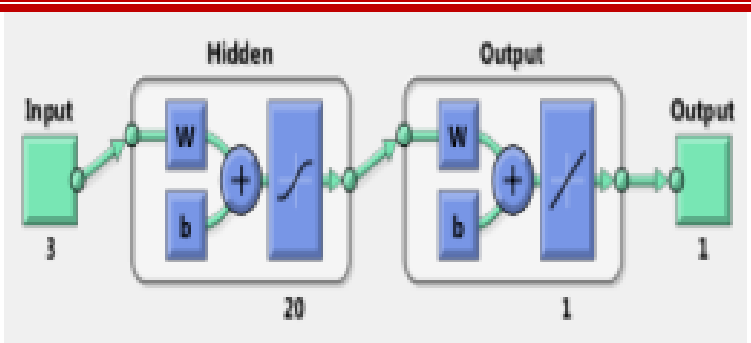

Fig. 3: ANN training Architecture

The best validation performance of 0.55259 achieved at epoch 6 as shown in Fig. 4 indicates that the ANN model converged rapidly to an optimal operating point during training. Such an early convergence at the minimum validation error implies that the network efficiently captured the temporal structure present in the impulsive noise data without prolonged training.

Further iterations beyond this epoch did not result in additional generalization gains, suggesting that continued training could result in overfitting. As such, network parameter selection at epoch 6 ensures a good balance between model prediction accuracy and generalization.

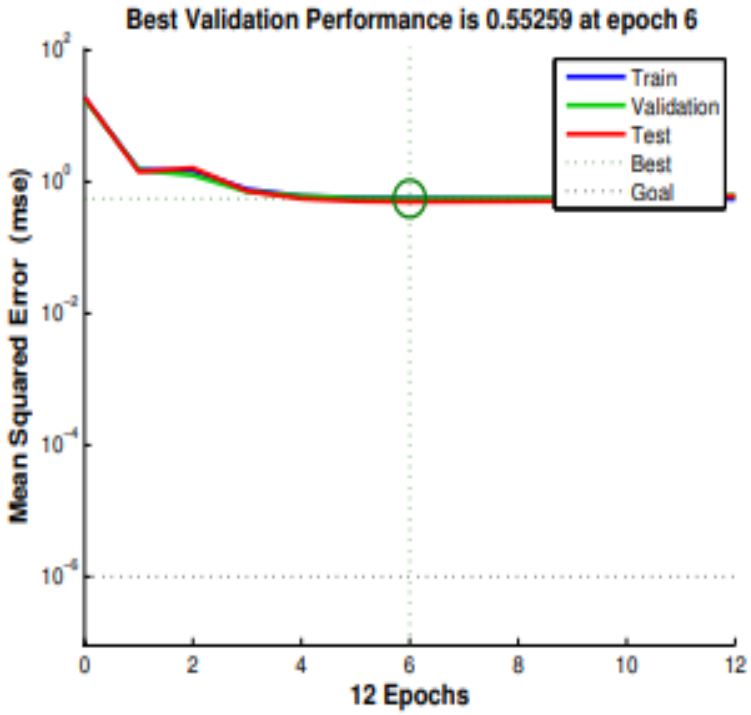

Fig. 4: Training performance plot

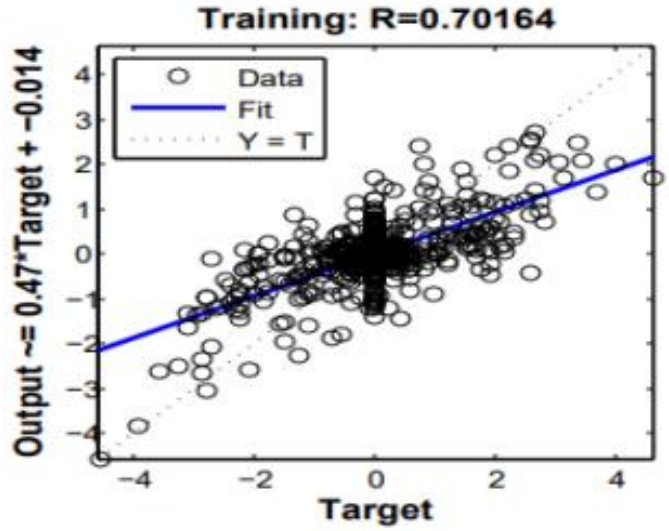

Fig. 5: Training regression plot

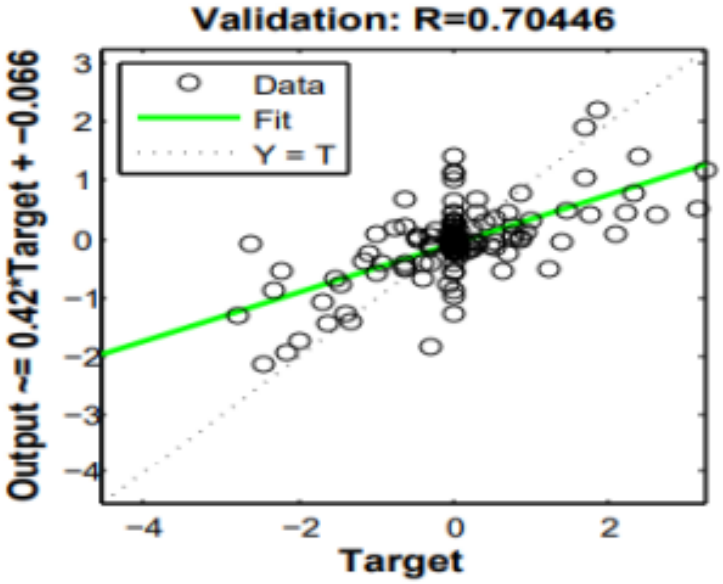

Fig. 6: Validation regression plot

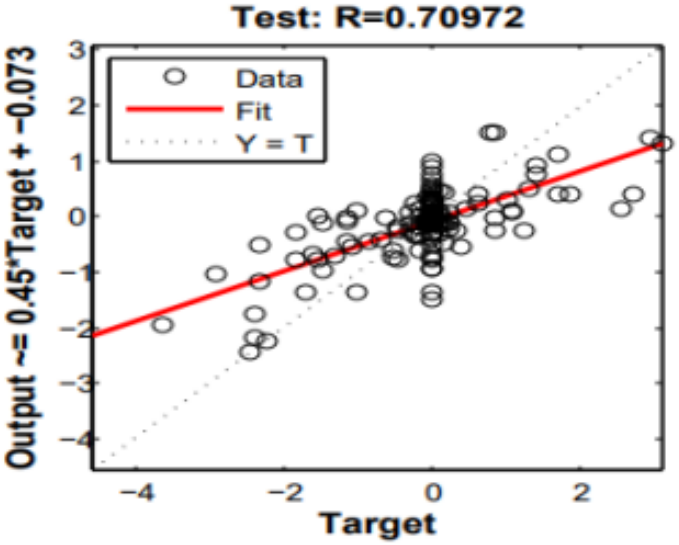

Fig. 7: Testing regression plots

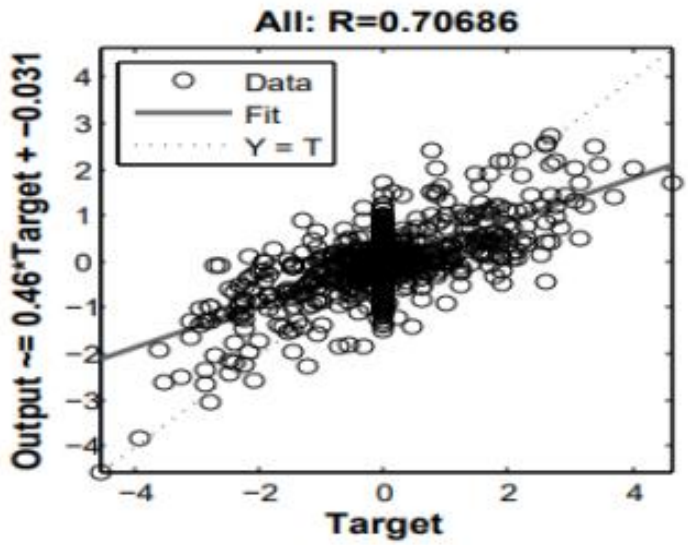

Fig. 8: All regression plot

The regression plots shown in Fig. 5, Fig. 6, Fig. 7 and Fig. 8 obtained from the trained ANN indicate a consistent and stable relationship between model output and measured impulsive noise data all through the data partitions. The training, validation, and test correlation values are clustered around 0.70, implying that the network has learned a generalizable mapping rather than overfitting to a specific partition of data. In addition, the slightly higher correlation seen in the testing phase also confirms the robustness of the realized model when unseen noise sample is introduced. In general, the aggregated regression result shows that the developed ANN model is bale to capture the dominant temporal patterns present in the measured impulsive noise while ensuring reliable predictive performance through the different operating conditions

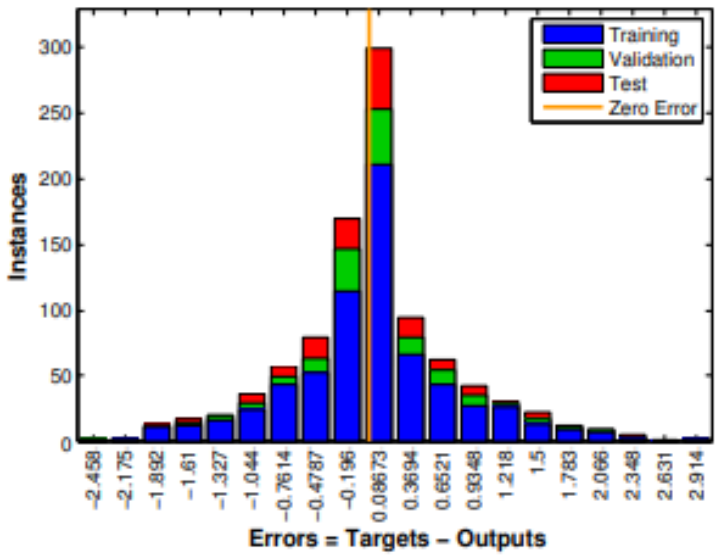

Fig. 9: Error histogram

Fig. 9 displays the error histogram of the trained ANN showing that majority of prediction errors are scattered around zero. This indicates close agreement between the model output and measured impulsive noise samples. The relatively narrow Fig. 6: Validation regression plot Fig. 7: Testing regression plots Fig. 8: All regression plot spread of the error distribution also shows stable learning characteristic with limited bias in the network output. Occasional larger errors correspond to high-amplitude impulsive events, which are inherently difficult to predict due to their abrupt nature. In general, this error histogram confirms the reliability of the proposed ANN model while maintaining robustness in the presence of high-amplitude and extreme noise events.

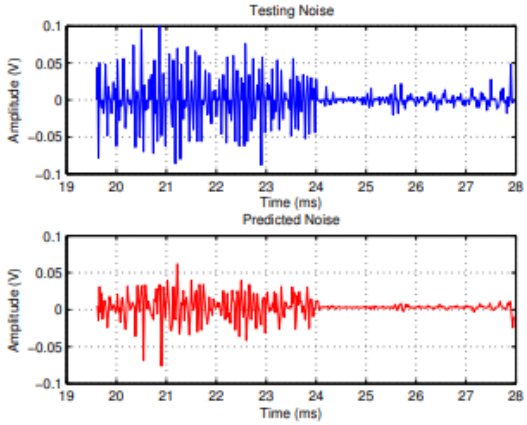

Fig. 10: Comparison of predicted and testing noise data

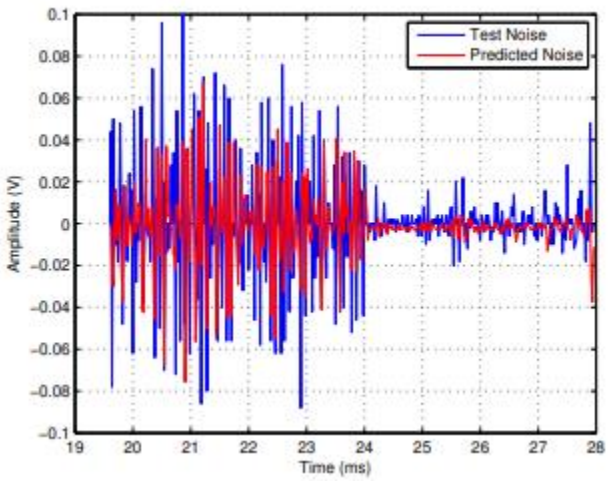

Fig. 11: Validation of predicted noise with measured noise

Fig. 10 and Fig. 11 presents comparison and validation plots of the model output and measured impulsive noise respectively. These results reveals a strong similarity in the temporal behaviour between the model output and measured impulsive noise, specifically in the timing and relative magnitude of dominant noise bursts. In the separate subplots in Fig. 10, the model

output signal closely follows the measured noise trend, demonstrating the ANN's ability to capture the underlying noise characteristics.

When both signals are overlaid on the same graph as shown in Fig. 11, the alignment of major peaks and transitions becomes more evident, showing how accurate the prediction is while also exposing the minor deviations in the abrupt impulsive events. These results confirms that the ANN captures the essential structure of the impulsive noise while maintaining consistent performance across different representations. A root mean square (RMSE) value of 0.77108 was realized indicating that the average deviation between the model output and measured impulsive noise data remained within a moderate and acceptable range in relation to the signal amplitude. Such a level of error shows the inherent difficulty of accurately forecasting abrupt and high-amplitude impulsive noise events in practical PLC networks. In spite of this challenge, this obtained RMSE confirms that the proposed ANN model provides a sufficient and meaningful approximation of the noise characteristic and is sufficiently accurate for supporting impulsive noise detection and selective suppression strategies

B. Suppression Results

The impulsive noise detection and suppression results displayed in Fig. 12 demonstrate how effective the proposed ANN model identifies sporadic noise impulsive events effectively and applies mitigation. By comparing the ANN-predicted noise against the defined threshold, the method successfully suppresses impulsive noise. The suppressed noise retains the overall structure of the measured noise while reducing the disruptive influence of impulsive components, indicating the effectiveness of the suppression process.

These results confirm that incorporating ANN-based prediction into the suppression process improves robustness against bursty impulsive noise while preserving signal integrity in indoor PLC networks.

6. Conclusion

In this study, an ANN-based framework for the detection and suppression of impulsive noise in indoor PLC network using measured noise data has been presented.

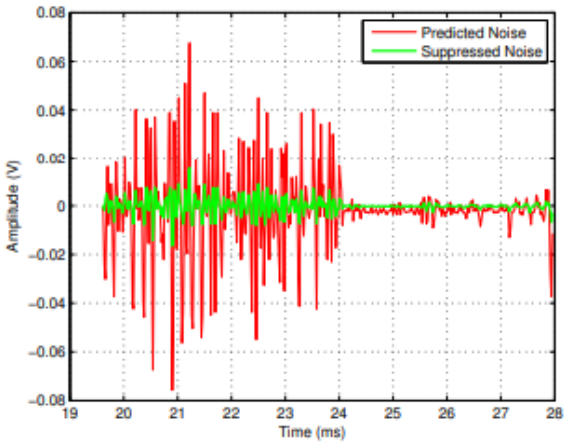

Fig. 12: Comparison of predicted noise with suppressed noise

By learning the short-term temporal characteristics of measured impulsive noise, the proposed feedforward ANN successfully predicts imminent noise samples that allows for suppression via a decision-based mechanism. The experimental results shows that this framework effectively and reliably identifies high amplitude impulsive events and suppresses their impact without incurring unwanted distortion to the underlying transmission signal. Contrary to the traditional fixed-threshold or linear techniques, the proposed approach herein adapts naturally to the nonstationary and nonlinear behaviour of practical PLC noise. In general, the results confirm that data-driven prediction generate a viable and flexible means of improving PLC system robustness, in particular to noise dominated indoor environments, and provides a basis for further integration with adaptive modulation and coding strategies.

7. References

[1] H. Meng, Y. L. Guan, and S. Chen, “Modeling and analysis of noise effects on broadband power line communications,” IEEE Trans. On Power Delivery, vol. 20, no. 2, pp. 630–637, 4 2005.

[2] M. Zimmermann and K. Dostert, “Analysis and modelling of impulsive noise in broad-band power line communications,” IEEE Trans. On Electromagn. Comp., vol. 44, no. 1, pp. 249–258, 2 2002.

[3] S. O. Awino, T. J. O. Afullo, M. Mosalaosi, and P. O. Akuon, “Time series analysis of impulsive noise in power line communication (PLC) networks,” SAIEE Africa Research Journal, vol. 109, no. 4, pp. 237–249, 12 2018.

[4] R. M. Vines, H. J. Trussell, L. J. Gale, and J. B. O. JR., “Noise on residential power distribution circuits,” IEEE Trans. On Electromagn. Comp., vol. EMC-26, 1984.

[5] D. Middleton, "Non-Gaussian noise models in signal processing for telecommunications: New methods and results for class A and class B noise models," IEEE Trans. On Inform. Theory, vol. 45, no. 4, pp. 1129–1149, 5 1999.

[6] ——, "Statistical-physical models of electromagnetic interference," IEEE Trans. On Electromagn. Comp., vol. EMC-19, no. 3, pp. 106– 127, 8 1977.

[7] M. Tlich, H. Chaouche, A. Zeddam, and F. Gauthier, "Impulsive noise characterization at source," in Proceedings of 2008 1 st IFIP Wireless Days (WD), 11 2008, pp. 1–6.

[8] G. Ndo, F. Labeau, and M. Kassouf, "A Markov-Middleton model for bursty impulsive noise: modeling and receiver design," IEEE Trans. On Power Delivery, vol. 28, no. 4, pp. 2317–2325, 10 2013.

[9] M. Antoniali, F. Versolatto, and A. M. Tonello, "An experimental characterization of the PLC noise at the source," IEEE Trans. On Power Delivery, vol. 31, 2016.

[10] C. R. Nokes, O. P. Haffenden, J. V. Mitchell, A. P. Robinson, J. H. Stott, and A. Wiewiorka, "Detection and removal of clipping in multicarrier receivers," European patent application EP1043874, vol. 4, pp. 785– 800, 10 2000.

[11] S. V. Zhidkov, "Analysis and comparison of several simple impulsive noise mitigation schemes for ofdm receivers," IEEE Transactions on Commun., vol. 56, no. 1, pp. 5–9, 2008.

[12] S. O. Awino, B. Nleya, and M. Molefe, "On the EVT-based nonlinear impulsive noise suppression over indoor low-voltage networks," in Proceedings of Southern Africa Telecommunication Networks and Applications Conference (SATNAC), 11 2025, pp. 324–328.

[13] S. O. Awino and B. Nleya, "Power line communication: Extreme noise events modelling and characterization over low-voltage networks," Progress In Electromagnetics Research C, vol. 162, pp. 242–251, 2025.

[14] R. Rojas, Neural Networks. A systematic Introduction. Berlin: SpringerVerlag, 1996.

[15] C. C. Aggarwal, Neural Networks and Deep Learning. Switzerland: Springer Nature, 2023.

[16] M. N. Ahuna, T. J. Afullo, and A. A. Alonge, "Rainfall rate prediction based on artificial neural networks for rain fade mitigation over earth satellite link," in 2017 IEEE AFRICON, 9 2017, pp. 579–584.

[17] S. Galli, A. Scaglione, and Z. Wang, "For the grid and through the grid: The role of power line communications in the smart grid," Proceedings of the IEEE, vol. 99, no. 6, pp. 998—-1027, 6 2011.

[18] Y. Chien, J. Chen, and S. Xu, "A multilayer perceptron-based impulsive noise detector with application to power-line-based sensor networks," IEEE Access, vol. 6, pp. 21 778—-21 787, 2018.

[19] M. Gotz, M. Rapp, and K. Dostert, "Power line channel characteristics and their effect on communication system design," IEEE Commun. Magazine, vol. 42, no. 4, pp. 78–86, 4 2004.

[20] S. O. Awino, T. J. O. Afullo, M. Mosalaosi, and P. O. Akuon, "On the application of periodic autoregressive models to PLC impulsive noise," in Proceedings of Southern Africa Telecommunication Networks and Applications Conference (SATNAC), 9 2019, pp. 328–333. [21] S. O. Awino and T. J. O. Afullo, "On the application of parsimoniuos periodic autoregressive models to bursty impulsive noise in low-voltage PLC networks," in 2021 IEEE AFRICON, 9 2021, pp. 1–5. [22] K. S. Al-Mawali and Z. M. Hussain, "Performance of bit-interleaved coded OFDM in power line communications with impulsive noise," in IEEE International Conference on Advanced Technologies for Communications, 10 2009, pp. 49–53.

Forensic Structural Audits and Remedial Interventions for Building Failure Resolution: Comparative Evidence from Two Reinforced Concrete Structures in Kenya

S. Murianka[1*], J. Ireri[2]

[1]Kirinyaga University, P.O. Box 143 - 10300, Kerugoya, Kenya.

[2]Civikraft Engineering, P.O. Box 102068, Nairobi, Kenya.

*Corresponding author: smurianka@kyu.ac.ke

Abstract

Building failures continue to pose severe safety, economic, and governance challenges in rapidly urbanising regions, particularly in developing economies where construction oversight systems remain inconsistent. Although deficiencies in design, construction execution, and geotechnical characterisation are frequently cited as contributing factors, empirical comparative forensic evidence distinguishing these failure mechanisms remains limited in Sub-Saharan Africa. This study presents a convergent mixed-method forensic structural investigation of two reinforced concrete buildings subjected to regulatory suspension in Kenya: (i) a completed multi-storey commercial residential building exhibiting widespread cracking, and (ii) a partially constructed institutional classroom block experiencing excessive slab deflection. Quantitative data were obtained through calibrated non-destructive concrete strength testing, geotechnical investigation, reinforcement verification, and finite-element structural simulation, complemented by qualitative visual inspection and construction documentation review. Results indicate that Case Study 1 experienced serviceability failure driven primarily by soil–foundation incompatibility, where a measured soil bearing capacity of approximately 131 kN/m² rendered the installed 2000 × 2000 mm column bases structurally inadequate despite satisfactory concrete strength (≈29 N/mm²). In contrast, Case Study 2 exhibited compounded serviceability and ultimate limit state deficiencies arising from under-strength concrete (≈76% of design strength), severe reinforcement under-provision (≈25% of design steel), and incomplete structural detailing. Remedial interventions were analytically designed and verified through structural simulation, including foundation underpinning and independent load-path augmentation. The findings demonstrate that building failure risk is governed not solely by material quality but by the integrity of geotechnical verification, execution governance, and professional supervision. The study provides empirically grounded guidance for forensic structural audits, remedial decision-making, and regulatory reform in developing construction contexts.

Keywords: Forensic structural audit; reinforced concrete failure; soil–structure interaction; non-destructive testing; structural remediation; construction governance.

1. Introduction

Structural failures in reinforced concrete buildings remain a widespread concern, particularly in developing economies. Building collapses occur in both developed and developing countries (Delatte, 2009). In Sub-Saharan Africa, factors such as rapid urbanisation, informal construction practices, fragmented regulatory oversight, and inconsistent professional supervision have contributed to a rise in building failures (Mwangi, 2026; Lagat *et al*., 2024; Kioko & Kimaiyo, 2023; NCA, 2020a). In Kenya, incidents of partial collapse, unsafe occupancy, and structural problems have increased over the past twenty years, raising serious questions about the effectiveness of current construction governance systems (NCA, 2024; NCA, 2020b; National Building Inspectorate, 2015). Building failures, whether total or partial, frequently result in injuries, loss of life, economic setbacks, diminished confidence in the construction sector, and stricter revisions of codes and procedures (Kioko & Kimaiyo, 2023; Delatte, 2009). The growing demand for housing and infrastructure—often driven by the need for affordable housing and further intensified by the shortage of housing units in urban centres—often pushes the construction industry towards missed deadlines or structural failure, especially when rapid delivery is prioritised over quality control and safety. This is reflected in the continually rising number of collapsed buildings, which currently exceed 100 projects.

The definition of building failure is far-reaching and confusing to most. In structural engineering, failure is broadly defined as the inability of a structure or its components to satisfy intended performance requirements under prescribed actions throughout its design life (Agudze *et al*., 2023). Such failure may occur at the serviceability limit state (SLS)—manifesting as excessive cracking, deflection, or settlement—or at the ultimate limit state (ULS), potentially resulting in collapse (Barrow, 2018). Importantly, many structural failures originate as serviceability deficiencies that are either ignored or inadequately addressed, subsequently escalating into life-threatening conditions.

Forensic structural engineering provides a systematic framework for investigating such failures through the collection, analysis, and interpretation of physical evidence, analytical data, and construction records. Structural audits, as a subset of forensic investigations, are increasingly employed by regulators to determine structural safety, assign responsibility, and guide remedial intervention (Feld & Carper, 1997). Contemporary forensic practice emphasises not only technical deficiencies but also governance-related factors, including the adequacy of supervision, quality control systems, and the completeness of documentation.

The American Society of Civil Engineers (ASCE) defines Forensic Engineering as the

application of engineering principles to investigate failures or other performance issues. Forensic engineering also involves giving testimony on the findings of these investigations in court or other judicial settings, when required. ASCE broadens the scope of forensic engineering by defining failures as follows: Failures are not always catastrophic, such as a building collapse, but also include facilities or parts of facilities that do not perform as intended by the owner, design professional, or constructor (ASCE, 2017). More simply described as "failure is an unacceptable difference between expected and observed performance" (Feld & Carper, 1997). Despite increasing interest in forensic engineering in Africa, most published studies remain descriptive case narratives with limited analytical depth, reproducibility, or comparative insight. Additionally, few studies clearly distinguish between geotechnical incompatibility and systemic execution failure as separate failure mechanisms, despite their fundamentally different remedial and policy implications.

This study addresses this gap by presenting a comparative forensic structural audit of two reinforced concrete building failures in Kenya. The objectives were to:
(i) diagnose root causes using triangulated quantitative and qualitative evidence;
(ii) distinguish soil–structure interaction failure from execution-governance failure mechanisms;
(iii) evaluate the adequacy of implemented remedial interventions through analytical verification; and (iv) derive implications for forensic engineering practice, professional oversight, and construction regulation.

2. Literature Review

Building failures are linked to various interacting factors, including design errors, material deficiencies, construction deviations, geotechnical uncertainty, and operational misuse. Studies in Europe and North America show that geotechnical factors constitute a significant part of structural distress cases, especially those involving excessive settlement and differential movement (Barrow, 2018). Conversely, research from developing economies often highlights poor workmanship, material substitution, and the lack of professional supervision as main contributors (NCA, 2020a). Forensic structural audits incorporate inspection, testing, and analysis to evaluate structural adequacy and failure causes. Agudze *et al*. (2023) suggest that assessing the structural integrity of existing structures may be necessary for reasons such as safety and/or serviceability impairments or deficiencies, or changes in the structures' intended functions. Depending on the type of structure and the client's brief, specific objectives of Structural Integrity Assessment may include, but are not limited to, developing a performance

report, establishing building use, serviceability, code compliance, life safety, durability, structural alterations, defects in design and construction, change of use or loading regime, and historic preservation (Ransom, 2005). Modern audits typically involve non-destructive testing methods, reinforcement verification, and analytical simulations to reconstruct as-built performance. International guidelines emphasise the need for objective diagnosis, separation of observation from inference, and explicit consideration of uncertainty.

Recent scholarship increasingly frames structural failure as a socio-technical phenomenon. The absence of qualified supervision, inadequate quality control systems, and weak regulatory enforcement have been shown to significantly increase failure probability (Lagat *et al*., 2024). In many developing contexts, construction governance remains skewed toward post-failure enforcement rather than preventive verification.

2.1 Research Design

A convergent parallel mixed-method design was adopted, integrating quantitative engineering diagnostics with qualitative forensic interpretation. Two case studies were investigated independently using identical methodological frameworks to ensure comparability.

2.2 Visual Inspection and Documentation Review

Systematic visual inspections were conducted to identify distress patterns, workmanship quality, and deviations from design intent. Approved structural drawings, material specifications, and available quality control records were reviewed to establish baseline design expectations.

2.3 Non-Destructive Concrete Strength Testing

In-situ concrete compressive strength was estimated using a calibrated Schmidt rebound hammer in accordance with **BS EN 12504-2**. Multiple readings were obtained per element, and calibration factors were applied to account for test orientation and surface condition. Results are reported as estimated mean values, acknowledging inherent uncertainty.

This was done to determine whether the concrete structural components, as built, met the intended design specifications.

Figure 1: Rebound Hammer used for concrete compressive strength tests (Source: Authors, 2025)

Any further tests are generally at the discretion of the supervising Structural Engineer (SE), based on observations, necessity, unforeseen in-situ conditions, the reliability of the employed methodology to provide sufficient diagnostic data, and the need thereof to proceed with additional diagnostic tests.

2.4 Geotechnical Investigation

Soil samples were obtained from foundation level and tested for plasticity index, shear strength, and density. Bearing capacity was estimated using classical bearing capacity theory and interpreted in accordance with Eurocode 7 principles.

2.5 Reinforcement Verification

Installed reinforcement was verified through direct measurement and comparison with approved drawings. Reinforcement adequacy was assessed based on sectional demand-capacity relationships.

2.6 Structural Modelling and Simulation

Finite-element structural models were created to assess as-built performance under code-mandated load combinations. Both serviceability and ultimate limit states were evaluated, with particular focus on deflection and the distribution of foundation stresses.

2.7 Ethical and Legal Considerations

All case data were fully anonymised. No identifying information regarding clients, contractors, or institutions is disclosed. Informed consent was obtained from relevant stakeholders, and the study is presented exclusively for scholarly and professional learning purposes.

3. Case Studies

The two case studies evaluated in this assessment are presented below. The structural investigation process is outlined, along with the diagnosis, conclusions, and recommendations.

3.1 Case Study 1: Five-Storey Commercial Residential Building Structural Failures

The commercial residential building was a ground-plus-five-storey structure. The building had been fully completed, demonstrating excellent materials and workmanship. However, before the handover, the owner noticed minor cracks on the masonry walls and several beams. The client requested the Structural Engineer (SE) to assess and advise on these issues. During the period while the SE was evaluating the structural integrity and providing a diagnosis, several days of rain occurred, worsening the failure.

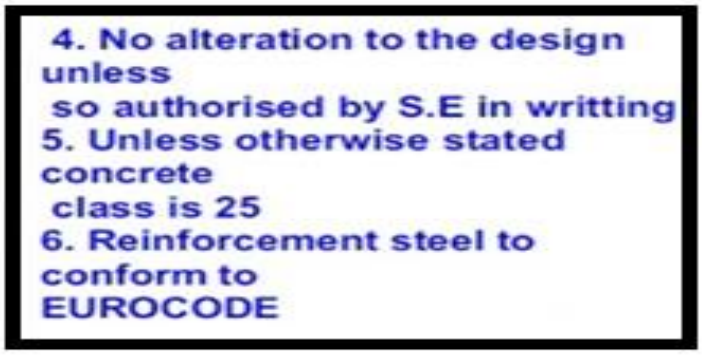

Figure 2: Excerpt from the approved structural drawings for Case Study 1 (Source: Authors, 2025)

The structural design drawings were reviewed to confirm the expected in-situ concrete compressive strength during construction. This was verified as Class 25, as shown in an excerpt from the approved structural design drawings (Figure 2). The next step was to assess whether the in-situ cast concrete achieved the required compressive strength.

Table 1: Case Study 1 Concrete compressive strength test results (Source: Authors (2025)

ITEM	STRUCTURAL MEMBER	NO. OF READINGS PER ELEMENT.	AVERAGE REBOUND READING	REBOUND HAMMER INCLINATION	CALCULATED ESTIMATIONS
1.	Column	40	30.03	90^0 horizontal	27.07 N/mm^2
2.	Beam	40	25.98	90^0 horizontal	23.42 N/mm^2
3.	Slab	30	32.57	90^0 upwards	26.82 N/mm^2
Average value obtained before calibration					25.77 N/mm^2
Rebound hammer calibration factor					1.13
Calibrated in-situ average compressive strength					29.12 N/mm^2

The rebound hammer test results obtained on site were compiled in Table 1. With an average of 29.12 N/mm², the concrete was confirmed to have exceeded the required design strength. Therefore, the structural failure was not related to strength but to other factors. Subsequent tests included soil analysis to assess the soil bearing capacity beneath the foundation. Samples of the masonry blocks from the superstructure walling were equally tested to test the ability of the constituent rock's compressive strength.

Table 2: Masonry block and Geotechnical test results (Source: Authors 2025)

ITEM	COMPONENT	TEST	RESULTS
1.	Masonry	Compressive strength	3.24N/mm^2
2.	Foundation Soil	Plasticity Index (PI)	25.8%
3.	Foundation Soil	Shear Capacity	24.8kN/m^2
4.	Foundation Soil	Sieve analysis	Poorly graded gravel with silt & sand.
5.	Foundation Soil	Dry Density	1350kgs/m^3
6.	Foundation soil	Bearing Capacity	130.94 kN/m^2

The masonry, with a compressive strength of 3.24 N/mm2 (Table 2), fell short of the acceptable minimum standard of 7.5 N/mm2 for load-bearing walls (BS 5628). Cracks in the masonry indicated failure under load, as the wall was subjected to forces exceeding its compressive strength capacity. The building was designed as a frame structure; the data confirmed that the design failed to achieve its intended purpose, despite the generally good workmanship of the reinforced concrete structural components.

The foundation soil analysis was also thoroughly assessed (Table 2). The failure was identified as purely geotechnical, as verified through tests carried out during the Forensic Structural Integrity Investigation. The soil beneath the foundation was found to be clayey gravel with a Plasticity Index of 25.8% and a Bearing Capacity of 130.9 kN/m². Further investigation, supported by simulation studies, showed that the bearing capacity and structure of the soil necessitated that the column bases measure at least 2900mm x 2900mm to support the load without failure or excessive settlement.

Figure 3: Differing soil strata leading to the contractor's erroneous decision (Source: Authors 2025)

The installed base size was instead 2000mm x 2000mm. It was further noted that the project contractor did not undertake testing of the soil bearing capacity but instead concluded the soil to be of adequate bearing capacity through visual inspection after excavating beyond the initial two (2) layers of seemingly much weaker soil (Figure 3). The colour of the third soil layer misled the contractor into adjudging it as soil of good bearing capacity.

Figure 4: Noted masonry cracks on Case Study 1 (Source: Authors 2025)

In Case 1, the key structural distress pattern observed was diagonal masonry cracks (Figure 4) on the walls of the majority of the building (25-30% of the walls). Confirmation from structural failure theory was sought to identify the corresponding failure cause.

The cracks were less than 2.0mm wide. According to Ransom (2005), visible cracks are a significant indication that the structure or parts of it are experiencing structural distress. Such a condition may be caused by:-

i. Error(s) in design;
ii. Error(s) in construction;
iii. Actual loading significantly in excess of design loading;
iv. Physical damage, impact, explosion, fire, etc.
v. Serious corrosion of reinforcement.

Table 3: Case Study 1 comparison of simulation data vs measured in-situ data (Source: Authors 2025)

ITEM	STRUCTURAL COMPONENT	APPROVED DRAWING DETAILING & INSTALLED	SIMULATION RESULT REQUIREMENTS	COMMENTS AND DEDUCTIONS
1.	Slab	D10 @ 200mm. Installed as expected.	D10 @ 250mm	The bars installed in-situ are more than adequate.
2.	Beams	5 No. D16 on Beams 1, 2 & 3; 4 No. D12 on Beam 4; 10 No. D16 on Beam 5; and 3 No. D20 & 2 No. D16 on Beam 6. Installed as expected.	Required adequate reinforcement was 6 No. D 16 based on the structural simulation of the most heavily loaded beam.	The project provided adequate reinforcement on beams.
3.	Columns	6 No. D20. Installed as expected.	6 No. D16 was the simulated requirement.	Project has demonstrated adequate sufficiency of the requirements on the column installation attribute.

ITEM	STRUCTURAL COMPONENT	APPROVED DRAWING DETAILING & INSTALLED	SIMULATION RESULT REQUIREMENTS	COMMENTS AND DEDUCTIONS
4.	Column base	Design and installation was 2000 x 2000 x 400mm column bases with D16 @ 200mm center to center.	Simulation indicates a column base of at least 2900 x 2900 x 400mm with D16 @ 200mm and 175mm center to center.	The project failed to provide column bases of adequate sizing based on the bearing capacity of the soil underlying the foundation.

The error was attributed to construction decision-making – failure to observe due diligence of geotechnical testing during execution. The consequence of this was settlement of the building. As the ground fell away, the weight of the building pushed the then suspended parts of the building down and the walls in that vicinity cracked. Cracking in such a situation is predominantly diagonal and follows the vertical and horizontal mortar joints in brickwork, unless the mortar is abnormally strong for the bricks used, where cracking occurs through the brickwork (Ransom, 2005).

Thus, the diagnosis was that cracking had been caused by settlement of the building due to inadequate soil bearing capacity and the consequent inadequate sizing of column bases commensurate to the low soil bearing capacity.

3.2 Case Study 2: Proposed Three-storey Classroom Block

During the client's routine inspection of the ground-floor and first-floor slab construction, excessive deflection was noted in the first-floor suspended slabs of the classrooms due to self-weight, while the structure was still under construction. This prompted the client to request the project's Structural Engineer for advice. The client had hitherto used a foreman as the site supervisor, construction manager, and Quality Control Manager. The need to have a Structural Engineer to oversee the structural works was not considered critical. The structural engineer, upon noticing the defects, notified the NCA, who halted the works and requested and structural integrity audit. This is the description of the audit under consideration.

The observed structural component distress was predicted to result from the failure of either concrete or reinforcement steel. Based on this premise, the compressive strength of concrete was measured, and the steel reinforcement was investigated. The first test was the measurement of concrete compressive strength using a rebound hammer (Table 4).

Table 4: Concrete Compressive Strength of the Classroom Block (Case 2)

ITEMS	STRUCTURAL MEMBER	NUMBER OF READINGS PER ELEMENT	AVERAGE REBOUND READING	REBOUND HAMMER INCLINATION	ESTIMATED IN-SITU COMPRESSIVE STRENGTH
1.	Columns	10	20.0	90^0 Horizontal	18.9 N/mm^2
2.	Floor Slab	10	20.9	90^0 Downwards	18.5 N/mm^2
Average value obtained before calibration					18.7 N/mm^2
Rebound Hammer calibration factor					1.05 N/mm^2
Calibrated in-situ average concrete strength					19.64 N/mm^2

Source: Authors (2025)

The compressive concrete strength of the failed suspended slab was confirmed to be 19.64 N/mm^2 (Table 4). This in situ concrete strength was less than the required design strength (Figure 5) by more than the recommended 85% (21.25 N/mm^2).

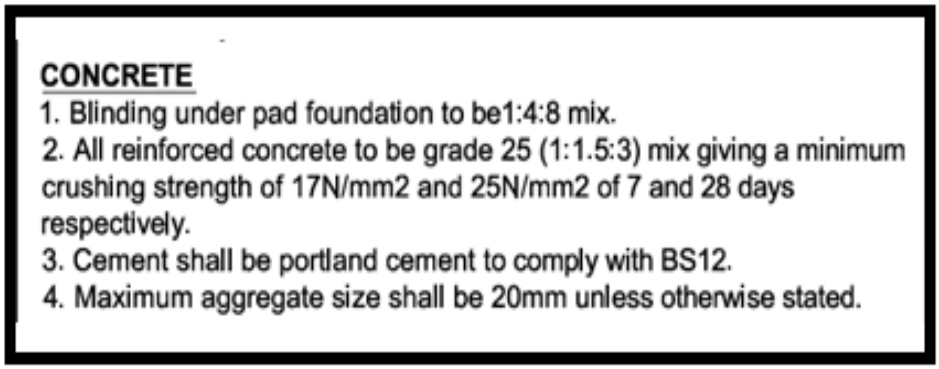

Figure 5: Excerpt from the approved structural drawings of Case 2 (Source: Authors 2025)

Thus, a partial explanation of the structural component distress or failure was the inability to achieve the required sufficiency of concrete compressive strength. The in-situ concrete strength was 92.42% of the absolute minimum required strength.

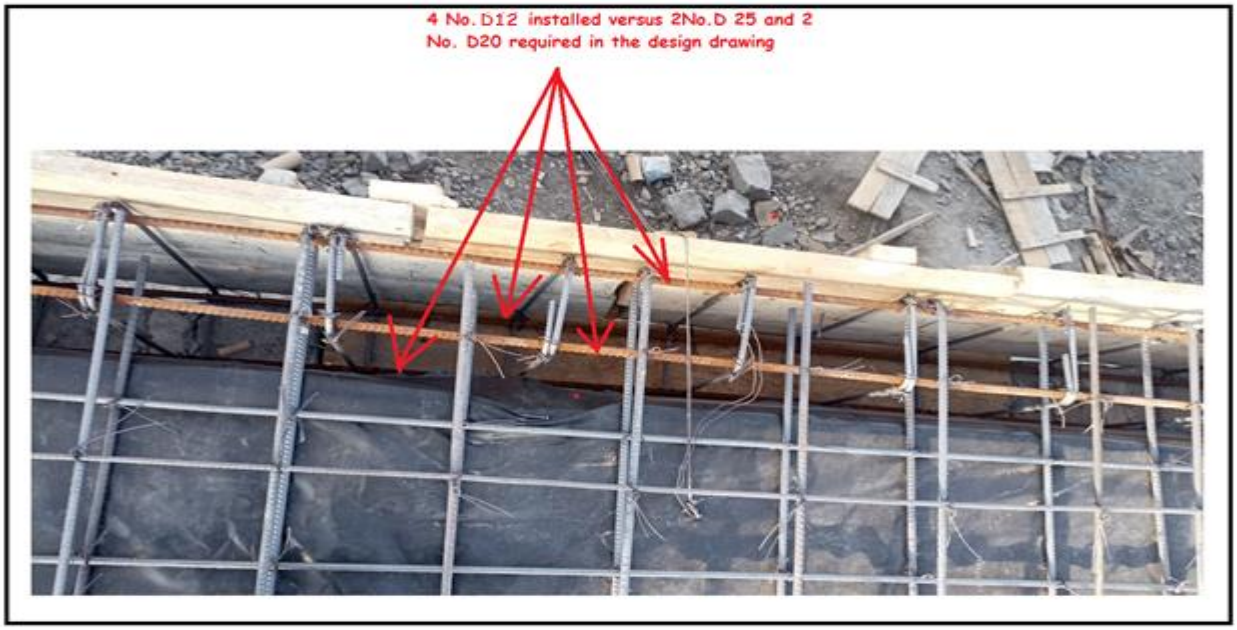

Figure 6: Case 2 -Installed beam reinforcement (4 No. D12)

Source: Authors (2025)

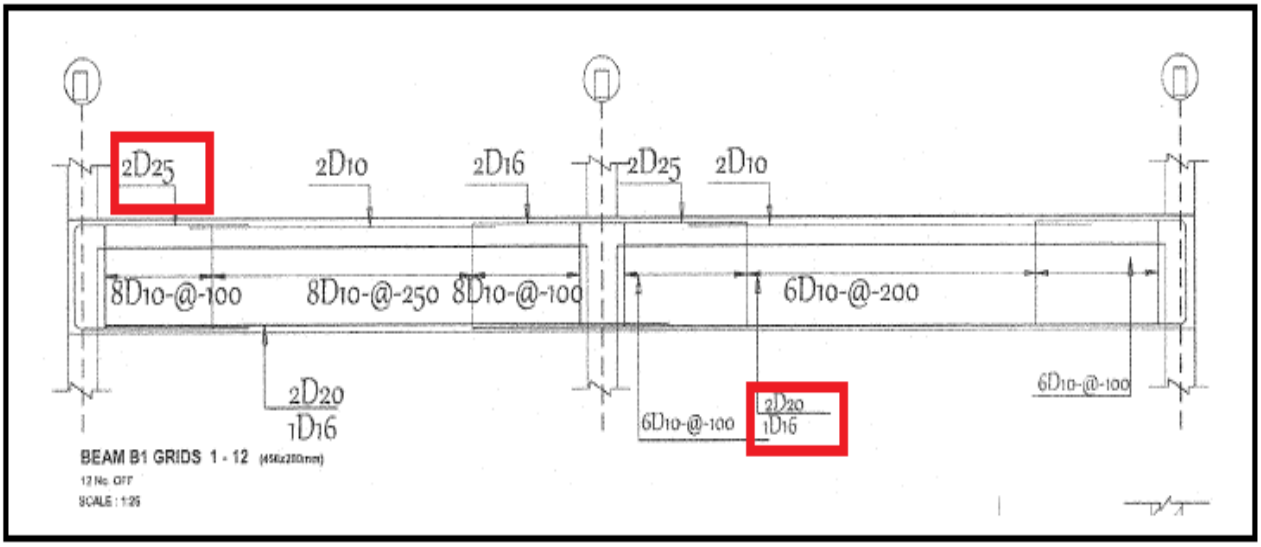

Figure 7: Case Study 2 - Design beam reinforcement

Source: Authors (2025)

Evaluation of the project execution photo narrative indicated that the installed reinforcement for critical structural components was substantially less than the design steel reinforcement - 4 no. D12 were installed on the concrete beam supporting the slab as opposed to the design recommendations of 2 No. D25 compression reinforcement and 2 No. D20 + 1 No. D16 reinforcement tension reinforcement. The installed steel reinforcement was 24.95% of the design requirement.

3.3 Evaluation of Structural Remedial Measures

A simulation using structural design software was conducted for Case Study 1 to determine the necessary retrofitting measures to remedy the noted failures effectively.

Figure 8: Structural members added as part of the retrofitting remedials

Source: Authors (2025)

Case Study 1: To arrest the ongoing settlement, additional columns with appropriately sized bases, considering the soil's bearing capacity, were designed and installed within the substructure through underpinning (portion of the remedial works shown in Figure 8). To distribute the load more evenly within the foundation, areas of concentrated loading were supported and buttressed using suitably reinforced concrete walls with strip footings compatible with the noted bearing capacity of the underlying soil. The enacted remedial action, based on the simulation results, significantly reduced the unit stress upon the soil, ensuring that the bearing capacity was not exceeded and preventing further shear failure and settlement.

Case Study 2: This project exhibited failures in several areas – inadequate quality of concrete, deficiencies in beam and slab reinforcement as well as absence of column base detailing on the structural drawings (Table 5). The Case Study 2 project exhibited multiple critical structural deficiencies at the superstructure level, indicating a fundamental collapse in quality control and execution supervision.

Table 5: Evaluation of the structural failures of Case Study 2 (Source: Authors 2025)

Deficient Attribute	**Quantitative/Qualitative Finding**	**Critique from Best Practice**
Concrete Quality	Average compressive strength 18.9N/mm^2 (76% of 25N/mm^2 required).	Failure of Material Quality Control: The site failed to use a proper mix design (recommended 1:1.5:3) and neglected mandatory cube crushing tests.
Beam Reinforcement	Less reinforcement installed as compared to design recommendations	Gross Execution Deviation: The on-site team dangerously substituted or omitted critical steel, leading to an under-reinforced condition.
Slab Deflection	Simulation showed deflection was more than (two 2) times the acceptable limit. Edge curtailment bar return length was less than design requirements.	Execution Error: The slab fails on serviceability (deflection) and strength at the support.
Omission of pertinent structural attributes on the structural design drawings	Column base details were missing from the structural drawings.	The column base, one of the most critical load-transferring elements was lacking from documentation, opening the door for arbitrary and unsafe construction.

Given these multiple, compounding failures (low strength, low steel, poor detailing), the required remedial measure was a Complete Structural Redesign and the implementation of new reinforced structural supports to correct deflection and restore load-carrying capacity.

Figure 9: Supportive beam added mid-slab as part of the retrofitting remedials

Source: Authors (2025)

Figure 10: Independent columns carrying mid-slab beam loading as retrofitting remedial

Source: Authors (2025)

Figure 11: Purchase of ready-mix concrete from a reputable supplier to assure quality control

Source: Authors (2025)

Specifically, a support beam was added across the centre of the first-floor slab (Figure 9), supported by external columns (Figure 10) that are independent of the existing failed structural components. Additionally, strict quality control measures were implemented for steel reinforcement installation and all concrete pours to ensure that the required Class 25 concrete was achieved in practice. This involved purchasing ready-mixed concrete (Figure 11) that met the specified requirements, rather than preparing concrete in situ.

4. Discussion

The forensic investigation of the two cases reveals a critical dichotomy in structural failure mechanisms: Case Study 1 represents a "high-quality failure" driven by design-geotechnical misalignment, while Case Study 2 represents a "systemic execution failure." These findings provide a nuanced understanding of the building crisis in Sub-Saharan Africa, challenging the common assumption that all failures stem from poor material quality.

4.1 The Geotechnical-Design Paradox (Case Study 1)

Case Study 1 demonstrated that even when material strengths exceed design specifications (29.12 N/mm² vs 25 N/mm²), structural integrity is not guaranteed. The failure resulted from a neglect to synchronize structural design with site-specific soil bearing capacities.

Global Context: This aligns with findings by Ratay (2000), who noted that foundation-related failures often stem from inadequate site investigations rather than structural member under-design.

Statistical Implication: The 31% deficit in footing area (2000mm X 2000mm vs 2900mm X 2900mm required) creates a concentrated pressure point that exceeds the ultimate limit state of the soil, rendering the superior concrete strength irrelevant. This highlights the necessity of a "Total System Reliability" approach in forensic audits.

4.2 Integrity Erosion through Material Substitution (Case Study 2)

Case Study 2 serves as a quintessential example of "deliberate non-compliance." The reduction of steel reinforcement by 75.05% and the 24.4% deficit in concrete strength represent a catastrophic departure from the "Limit State Design" philosophy.

Root Cause Analysis: Unlike Case Study 1, where the error was technical/judgmental, Case Study 2 points to a failure of professional ethics and site supervision. As noted by Senteu *et al.* (2014), the absence of consistent, third-party inspection in Nairobi and its environs creates a "regulatory vacuum" where contractors prioritize cost-saving over structural safety.

Forensic Diagnostic Value: The use of NDT (Rebound Hammer and Rebar Scanning) was pivotal in Case Study 2. In high-impact journals, this underscores the move toward *Quantitative Forensic Engineering*, where visual distress is merely the starting point for a data-driven diagnosis.

4.3 Comparative Implications for Forensic Practice

The comparison suggests that forensic audits must be multidimensional. If the audit for Case Study 1 had focused solely on concrete strength (a common practice in basic audits), the building would have been cleared, despite being fundamentally unsafe due to its foundation. Conversely, Case Study 2 demonstrates that "visual beauty" can mask systemic internal weaknesses.

5. Conclusions

This research leads to the following conclusions regarding the resolution of building failures in rapidly urbanizing regions:

1. Divergent Failure Pathologies: Building failures are not monolithic. They range from discrete technical oversights (geotechnical mismatches) to systemic material deficiencies. Forensic protocols must therefore be standardized to include mandatory geotechnical verification and NDT scanning regardless of the "apparent" quality of workmanship.

2. Reliability of NDT in Forensic Audits: The Schmidt Rebound Hammer and rebar scanning provided a high degree of correlation with observed structural distress, validating their role as indispensable tools for rapid structural integrity evaluation in resource-constrained environments.

3. The Oversight Deficit: The analysis of Case Study 2 confirms that the primary driver of execution-based failure is the circumvention of professional supervision. The structural integrity of a building is as much a product of "regulatory adherence" as it is of "engineering design."

6. Recommendations

6.1 For Policy and Regulatory Frameworks

Mandatory "As-Built" Certification: The National Construction Authority (NCA) should mandate a "Forensic Close-out Report" for all multi-storey buildings. This report must include NDT test results and a geotechnical verification signature, ensuring the "as-built" matches the "as-designed" parameters.

Digital Material Traceability: Implementing a blockchain-based or digital log for concrete pours and steel procurement can mitigate the unauthorized material substitutions observed in Case Study 2.

6.2 For Engineering Practice

Geotechnical-Structural Integration: Structural engineers must refuse to issue structural completion certificates without a verified site-specific soil report. The practice of assuming a "standard" bearing capacity must be legally discouraged.

Adoption of Remedial Redundancy: As seen in the remediation of Case study 2, when systemic failure is detected, the introduction of independent structural systems (e.g., external steel frames or independent columns) is preferred over simple patching, as it bypasses the "unknown" reliability of the existing failed members.

6.3 For Future Research

Further study is required to develop a Structural Integrity Risk Index (SIRI) for Sub-Saharan Africa that weights geotechnical risks, material quality, and supervision levels to predict the likelihood of collapse before visual distress becomes apparent.

References

Agudze, S., Akortia, V. K., Kankam, C. K., Biney, E., Quarm, J. K. & Mansr, E. C. (2023). Appraisal of Structural Integrity Assessment Methodology and Reporting of Existing RC Building Structures in Ghana, *Journal of Engineering Research and Reports*, 25(10), 81-101. ISSN: 2582-2926.

ASCE. (2017). "Forensic engineering." Accessed January 10, 2026. http://www.asce.org/forensicengineering/

Assakkaf, I., Sakka, Z. & Qwazeeni, J. (2016). Structural Assessment and Reliability of Existing Building. *Asian Pacific Symposium on Structural Reliability and its Applications (APSSRA6)*.

Atkinson, M. F. (2004). Structural Foundations Manual. Spon Press, London, UK.

Barrow, R. S., Anthony, R. W., Beasley, K. J., & Verhulst, S. M. (2018). Guidelines for Failure Investigation. American Society of Civil Engineers (ASCE). Virginia, USA.

Darwin, D., Dolan, C. W. & Nilson, A. H. (2016). Design of Concrete Structures, 5th Ed. McGraw Hill Education, New York, USA.

Delatte, N. J. (2009). Beyond Failure – Forensic Case Studies for Civil Engineers. American Society of Civil Engineers (ASCE) Press, Virgini, USA. ISBN 978-0-7844-0973-2.

Feld, J., and Carper, K. (1997). Construction Failure. 2nd Ed. New York: Wiley.

Kioko, J. & Kimaiyo, F. (2023). Tackling the Recurrent Collapse of Buildings in Kenya. The Kenya Institute for Public Policy Research and Analysis (KIPPRA), Nairobi. Retrieved on January, 10, 2026 from https://kippra.or.ke/tackling-the-recurrent-collapse-of-buildings-in-kenya/

Lagat, D., Kivaa, T., Njuguna, M., Nyakondo, S., Maklago, E., Onkangi, R., Kamulla, C. & Kimathi, B. (2024). Factors Affecting The Physical and Functional Performance of Buildings in Kenya, *Journal of The Kenya National Commission for UNESCO*, 4 (1), 1 – 20. https://doi.org/10.62049/jkncu.v4i1.72

Mwangi, A. (2026, January, 6) Poor Quality Construction Materials Fuel Kenya's Building Collapse Crisis, Business Daily. Retrieved on January 10th from https://share.google/DIvuUCgKmrRZECjrS

National Building Inspectorate (2015). *Building Audit Report*. Nairobi.

NCA (2024). Construction Industry Outlook 2024. National Construction Authority (NCA). Nairobi, NCA. https://www.nca.go.ke:81/media/FINAL_CIO_20.11.25.pdf

NCA. (2020a). Research on Failure and Collapse of Buildings in Kenya. National Construction Authority (NCA). Nairobi: NCA. ISBN: 978-9914-9856-0-3. Retrieved on January, 10, 2026 from https://www.nca.go.ke/media/RESEARCH_on_Building_Faillures_.pdf

NCA (2020b). Construction Industry Outlook in Kenya: Industry Statistics and Trends – 2020. National Construction Authority (NCA). Nairobi, NCA. Retrieved on January, 10, 2026 from https://www.nca.go.ke/media/Construction_Industry_Outlook_-_1st_Edition.pdf

Noon, R. K. (2001) Forensic Engineering Investigation. CRC Press. London, UK.

Ransom, W. H. (2005). Building Failures: Diagnosis and Avoidance. Taylor & Francis, London, UK.

Ratay, R. T. (2000). Forensic Structural Engineering Handbook. The McGraw Hill Companies Inc., USA.

Senteu, A., Mugwima, N. & Kivaa, T. (2014). The Influence of Construction Inspection on Building Quality: The Case of Nairobi City, Kenya. *African Habitat Review Journal (AHR), 8, 1-17.* Available on https://www.academia.edu/39827096/THE_INFLUENCE_OF_CONSTRUCTION_INSPECTION_ON_BUILDING_QUALITY_THE_CASE_OF_NAIROBI_CITY_KENYA

Shikh, M. F., Pthak, R. & Pndey, A. (2020). Forensic Study and Review of some Structural Failures – Case Studies. *International Journal of Technical Innovation in Modern Engineering & Science (IJTIMES)*, 6(1), 9 -18. E-ISSN: 2455-2585

Loss Reduction Strategy in a Distribution Network: A Case Study of Rhino Park 11kV Line in Nairobi, KENYA

K. Wachira[1*], D. R. Segera[2], K. D. Njoroge[3], L. O. Angira[4], V. M. Michiira[5]

[1, 4, 5] KPLC, Kenya

[2, 3] University of Nairobi, Kenya

*Corresponding author: engkahorowachira@gmail.com

Abstract

A power distribution network is required to provide quality and reliable power supply for its customers connected to it. In the Kenyan system, there has been a great need to ensure that the cost of power distribution is reduced to the extent that it meets global standards. This ensures that the cost of electricity distribution is minimized, thereby ensuring competitive operational expenditure cost following the initial capital expenditure spent on its development. The paper has laid the groundwork by studying the impact of losses brought about by the main components contributing to losses in power line infrastructure, namely distribution lines and power distribution transformers.

The loss reduction optimization strategy adopted and simulated, has indeed shown a marked loss reduction by optimization, resulting in a significant cost reduction by extension, a marked long-term positive impact on the distribution grid.

Keywords: Loss reduction, Optimization strategy, Distribution, Optimization, NEPLAN

1. Introduction

The electrical power distribution network is the backbone of any power system because it is the critical link between power transmission from generation stations and the customer end through the energy meter. The efficiency of power systems directly impacts the reliability and cost of electricity supplied to consumers [1]. The demand for electrical power has increased over the years due to increased urbanization coupled with an aggressive government policy on electrification, not only in the city of Nairobi, but across Kenya. The growth of economic and social activity in the Nairobi cosmopolitan area has also significantly added pressure on the already existing power distribution network.

A combined loss reduction approach to having an efficient distribution network will enable the power system to run smoothly while reducing energy wastage [2]. In addition, the measures

will reduce operational cost and improve the overall reliability of the power system in the country.

The power industry has undergone several transformations due to technological advancements and the need for clean energy [3]. These changes have sparked a debate on ways to minimize losses in electricity distribution networks. Technical energy losses in distribution networks have become rampant, especially in distribution lines and transformers [2]. That is mainly due to load current and conductor resistance [4]. These losses are caused by the aging of power line conductors, natural deterioration of hardware accessories and the time taken attending to distribution system breakdowns which affects the time required to carry out line inspections and maintenance proactively before a breakdown occurs.

On the other hand, non-technical losses have stemmed from direct electricity theft coupled with metering and billing challenges [5]. Solving these problems step by step requires integrating new approaches that enhance Kenya's electrical power supply quality and reliability for customers.

Figure 1 below provides a visual representation of some of the areas of loss optimization: distribution lines, and power transformers.

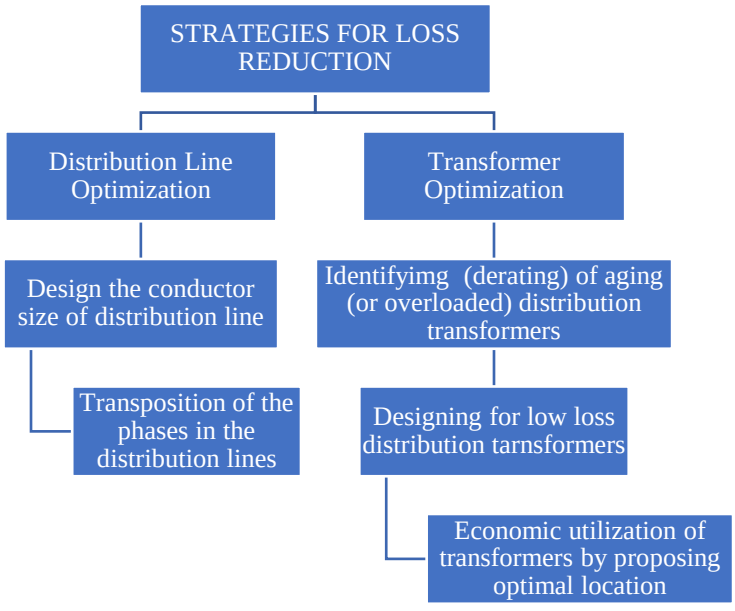

Figure 1: Strategies for loss reduction considered in this study

The main objective of this paper is to investigate and redesign an optimized approach for reducing losses in an electrical distribution network using an integrated loss reduction strategy in Kenya's power system in Nairobi. The study will target an installed 12km 11kV power distribution line feeder known as 'Rhino Park Ex-Dagoretti', which has 30 three-phase power distribution transformers of various capacities.

In the evaluation of losses in the distribution lines of the network, consideration of the design of the network using different conductor sizes available will be looked at as specified in the company's design and construction standards and specifications. Coupled with this, it will be essential to see if the transposition of the 11kV distribution network will have any significant impact on losses.

Coming to the distribution transformer losses in this strategy, this research has factored in the transformer technical allowable losses (no-load and full load). There is the impact of transformer aging, the use of low-loss equipment, de-rating, and the economic utilization of the transformers already installed in the distribution network will affect loss and if the data is readily and adequately available.

Figure 1 above depicts the proposed areas for examination when carrying out the power loss optimization strategy. Each of the areas has been considered with a view to assess its viability from both an energy-saving and cost-saving perspective.

With regard to areas of consideration when looking at the distribution network lines, the study will be considering the impact of a change in the conductor size and transposition of the 11kV distribution network under consideration. When we focus on optimizing the distribution transformers on the network, the study will review the opportunity for transformer loss optimization by considering the impact of aging transformers and the need for de-rating of transformers based on loading and the number of years of operation. The consideration for replacement of the traditional CRGO (core rolled grain oriented) core type transformers existing in the distribution network with the new technology low-loss amorphous core transformers requires some discussion. The location of the distribution transformers in the network, as designed, plays a significant role in loss reduction and will be looked into. It is essential to note that the study location area is in the outskirts of the city of Nairobi, and the line follows both the classified road network and the land use profile characteristic of small-scale domestic households, with the occasional residential estate.

To determine the approach to take when assessing the use of various loss reduction optimization strategies, the study has considered the loss optimization initiatives that have the significant positive impact. When we look at the initiatives for change of conductor size, we shall be analysing the load profile and losses associated with the existing network overhead conductor size of 75mm2 against the losses associated with the increase in the conductor cross-sectional area of 150mm2. The choice of this conductor size is governed by the global standards of manufactured conductor sizes for power distribution networks. Table 1 below

shows the technical characteristics of the two conductor sizes. The underground cable take-off portion of the 11kV distribution line for this study has no impact on the loss reduction optimization calculations due to its short length, large cross-sectional area, and close proximity to the primary substation where the 11kV distribution line is connected.

Table 1: Electrical parameters for cable and conductors under consideration in the distribution line feeder

(Source: Manufacturers design specification (2025))

Type	R(0) Ohm/km	X(0) Ohm/km	C(0) uF/km	Unit	Urk V	Q mm²	Rated Temp °C	Operating Temp. °C	Max. Temp. °C
300mm² Single core XLPE cable (Al)	0.164	0.079	0.47	km	11	300	20	40	80
Horizontal 150mm² ACSR conductor (Al)	0.371031	1.857342	-	km	11	150	75	75	75
Horizontal 75mm² ACSR conductor (Al)	0.590031	1.886324	-	km	11	75	75	75	75

Table 2: Symbol Description

Symbol	Description	Unit
Type	The type of cable or conductor under consideration (e.g., "300mm² Single core XLPE cable (Al)" or "Horizontal 150mm² AND 75mm² ACSR conductor (Al)").	-
R(0)	Zero-sequence resistance, representing the resistance per unit length in a balanced three-phase system under zero-sequence conditions (used in power system fault analysis).	Ohm/km
X(0)	Zero-sequence reactance, representing the inductive reactance per unit length in a balanced three-phase system under zero-sequence conditions.	Ohm/km
C(0)	Zero-sequence capacitance, representing the capacitance per unit length to ground or between phases in zero-sequence conditions (typically for cables; blank for overhead conductors).	µF/km
Unit of Length	The reference unit length for the electrical parameters (R(0), X(0), C(0)).	km
Ur	Rated voltage of the cable or conductor.	kV
Q	Cross-sectional area of the conductor (Q likely denotes "Querschnitt" or similar, but interpreted as conductor size).	mm²
Rated Temp	Rated temperature, the maximum temperature the insulation or conductor is designed to withstand continuously under normal operating conditions.	°C
Operating Temp.	Operating temperature, the typical or design temperature during normal service.	°C
Max. Operating Temp.	Maximum operating temperature, the highest temperature the conductor or cable can safely reach without extreme sagging or breach of clearance (often during overload or fault conditions).	°C

The 11kV distribution line length is made of sections or nodes, and the layout is considered to be radial for the evaluation of the loss along its length. For the flexibility of the network, there are open points where the isolators are left in the normally open position. Figure 3 below shows the single line diagram which includes the distribution transformers in the network.

Figure 2 below shows the 30 no. distribution transformers that have been considered in this study as the currently existing equipment of varying power ratings. One additional transformer of 1,000kVA, which had been part of the network, has since been decommissioned and removed from the distribution network. This is because the customer that was previously served no longer consumes electricity and has shut down their operations.

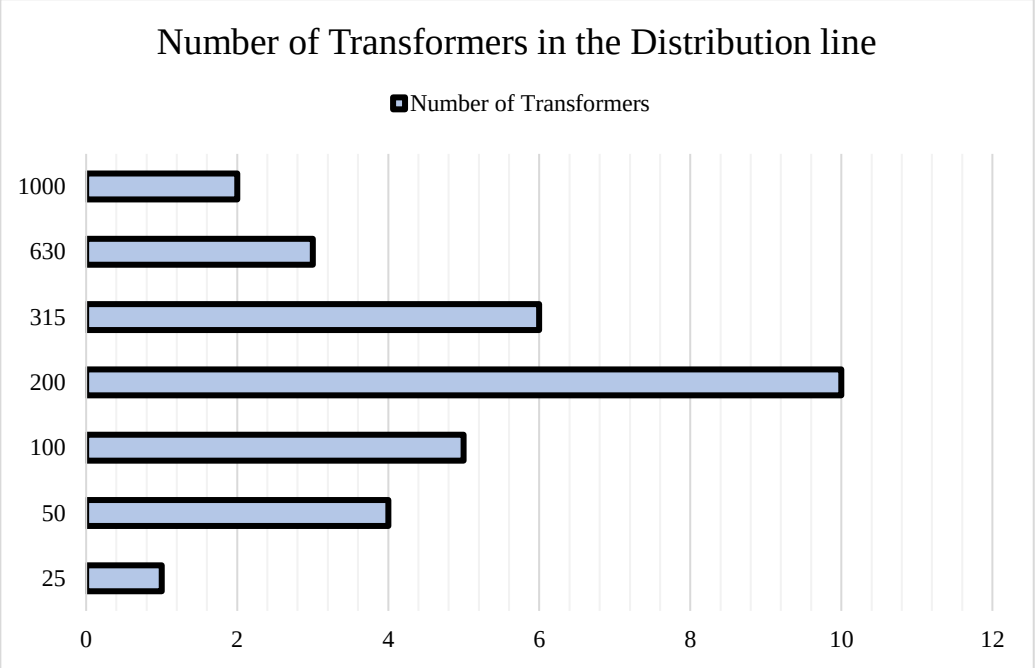

Figure 2: Number of transformers by kVA rating installed in the distribution line feeder

2. Methodology

The research has used a modeling process that has involved the detailed representation of the distribution network's key components, that is, the distribution lines, power transformers, and load points.

The distribution lines have been modeled using two scenarios, using 75mm² and 150mm² aluminum conductors, with their electrical parameters (resistance, reactance, and susceptance) defined based on manufacturer specifications and KPLC design and construction standards. Additionally, the power transformer's power rating, no-load losses, and load losses will be incorporated into the model to reflect their operational impact on the loss reduction strategy.

Load points will be represented using actual KPLC daily load data over a period of one month, capturing the demand profile, efficiency, and voltage variation across the length of the 11kV distribution feeder in this research study.

The model of loss reduction optimization has been validated by comparing scenario-based optimization strategy simulation results with KPLC's operational data. Consideration for any discrepancies will be addressed by refining the loss reduction strategy model parameters to achieve alignment with the actual power system performance dynamics.

3. Results

The design of the single line diagram of all the electrical elements in the distribution system were modelled and simulated using NEPLAN software.

Figure 3 below depicts the complete network modeled using the software for simulation. This diagram represents the complete Rhino Park 11kV Power Distribution Line Feeder network. It includes all 30 distribution transformers along with their respective loads, power lines, and electrical components. The network is fully modelled with the requisite electrical equipment, design specifications, and electrical characteristics applied. Running simulations on this section of distribution network under study provides insights into its performance and optimization potential. This full schematic shows the overall structure of the distribution system and how each component interconnects.

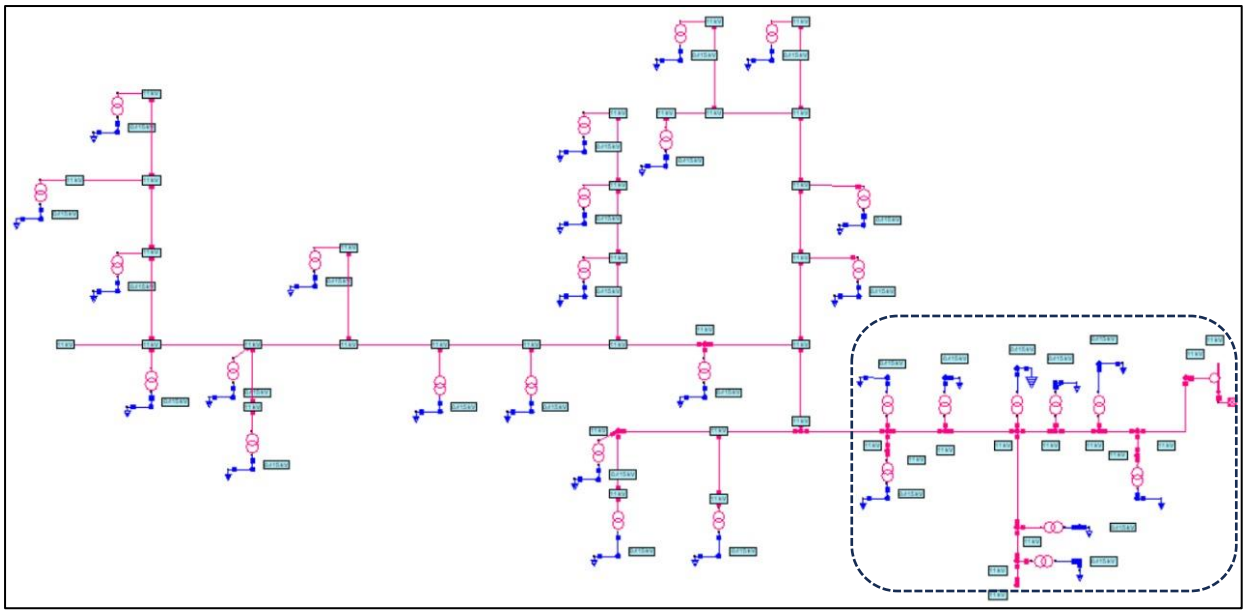

Figure 3: Complete single line diagram (SLD) of Rhino Park 11kV Power Distribution Line Feeder

Table 3 shows the symbols representing the various sections of the SLD of figure 3 above

Symbol	Description
	Dagoretti Sub-station 11kV Busbar
	Power Measuring Instrument
	Section of 11kv distribution network expanded in figure 4
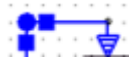	Customer Load
	Power Transformer
	Distribution line Label

Figure 4 below shows the NEPLAN schematic diagram showing the 11kV source busbar from where the distribution feeder originates. This is a section of the entire network under consideration. The complete schematic diagram modelled with the requisite electrical equipment, modelled and design specifications for electrical characteristics applied to the network. This diagram zooms into a specific section of the complete network depicted in Figure 3 above. It shows the 11kV source bus, from which the distribution feeder starts. This section includes the 30 distribution transformers, the associated power lines, and the interconnected loads within this part of the network. The focus here is on the specific electrical characteristics and equipment used in this area. It is from this section that simulations were run to assess system loss reduction optimization and to evaluate the performance of this part of the power distribution system under study.

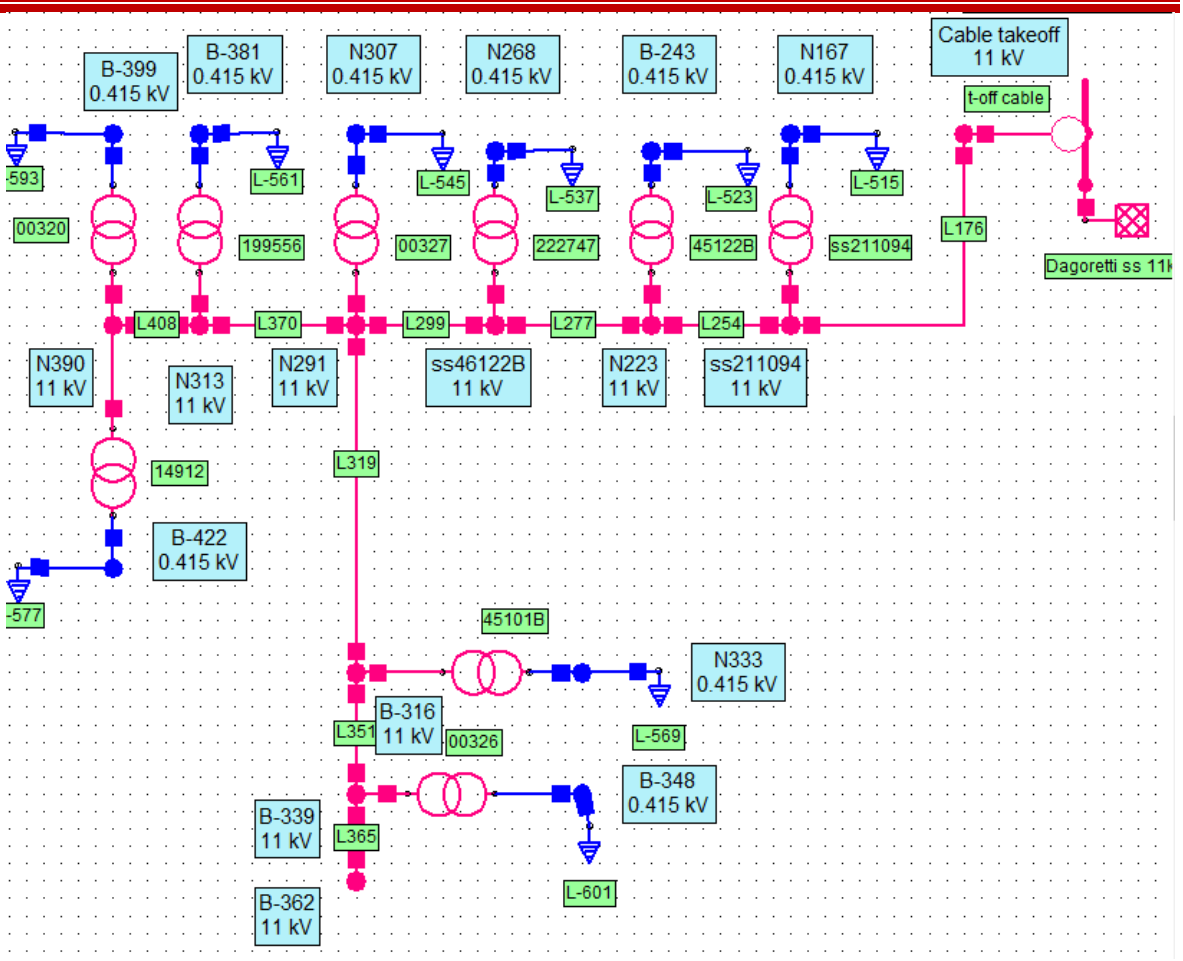

Figure 4: Partial single line diagram of Rhino Park 11kV Power Distribution Line Feeder

Incorporating the 30 distribution transformers with the loads, along with the power lines, to build the entire distribution network under study and running a simulation will provide results that, when analyzed, will provide the answer to the level of optimization of the system achievable.

A first loss reduction optimization model for simulation has been developed using two conductor sizes to examine the power losses. The electrical parameters for the two conductors under consideration are as defined in Table 4 below. The transformer locations and losses were set using standard acceptable losses as obtained by KPLC data for all sizes used in this simulation. Power loss optimization of the transformers in terms of capacity and location has been achieved primarily because their location has been limited to the wayleave access and use of road reserve corridors, which are already predetermined in the country's land use and urban planning policies.

Table 4: Electrical characteristics of the distribution feeder with standard conductor sizes

Conductor size	**R(0)** (ohm/km)	**Length** (km)	**Total R** (Ohms)
75 mm^2	0.590031	12	7.08
150 mm^2	0.371031	12	4.45

Table 5: Symbol Description

Symbol	**Description**	**Unit**
Conductor size	The cross-sectional area of the conductor.	mm^2
R(0)	Zero-sequence resistance per unit length in a balanced three-phase system under zero-sequence conditions.	ohm/km
Length	The length of the conductor segment.	km
Total R	The total resistance calculated as R(0) multiplied by the length.	Ohms

3.1. Results of loss reduction strategy optimization in energy units

The analysis of optimization results involves a detailed comparison of loss reduction, cost savings, and reliability improvements across the various scenarios simulated in NEPLAN. The focus will be on key electrical parameters, including voltage, current, impedance, and power. Each scenario represents different combinations of loss reduction strategies, which will be evaluated to quantify their impact on technical and non-technical losses.

Voltage profiles will be analyzed to assess improvements in power stability and regulation, while current flow has been evaluated to confirm a reduction in line and power losses. Impedance data, derived from increased conductor size and review of transformer parameters, have been used to validate loss reduction calculations. Following the simulation, the use of the $75mm^2$ conductor gives a loss of 1.7% compared to the use of the 150mm2 conductor of 1.5%. This is a 0.2 percentage point reduction in losses. Tables 6 and 7 below show the losses following simulation using the NEPLAN software, and additional data of the feeder meter located in the substation, and data collected over one month every 15 minutes.

Table 6: Loss computation for use of the distribution feeder with existing $75mm^2$ conductor size

P Loss MW	**Q Loss** MVar	**P Imp** MW	**Q Imp** MVar	**P Gen** MW	**Q Gen** MVar	**P Load** MW	**Q Load** MVar	**Iron Losses** MW	**Losses ($75mm^2$ conductor)** %
0.024	0.009	1.392	0.228	1.392	0.228	1.368	0.219	0.017	1.7%

Table 7: Loss computation for use of the distribution feeder with existing 150mm^2 conductor size

P Loss MW	**Q Loss** MVar	**P Imp** MW	**Q Imp** MVar	**P Gen** MW	**Q Gen** MVar	**P Load** MW	**Q Load** MVar	**Iron Losses** MW	**Losses (150mm^2 conductor)** %
0.021	0.008	1.392	0.228	1.392	0.228	1.371	0.22	0.017	1.5%

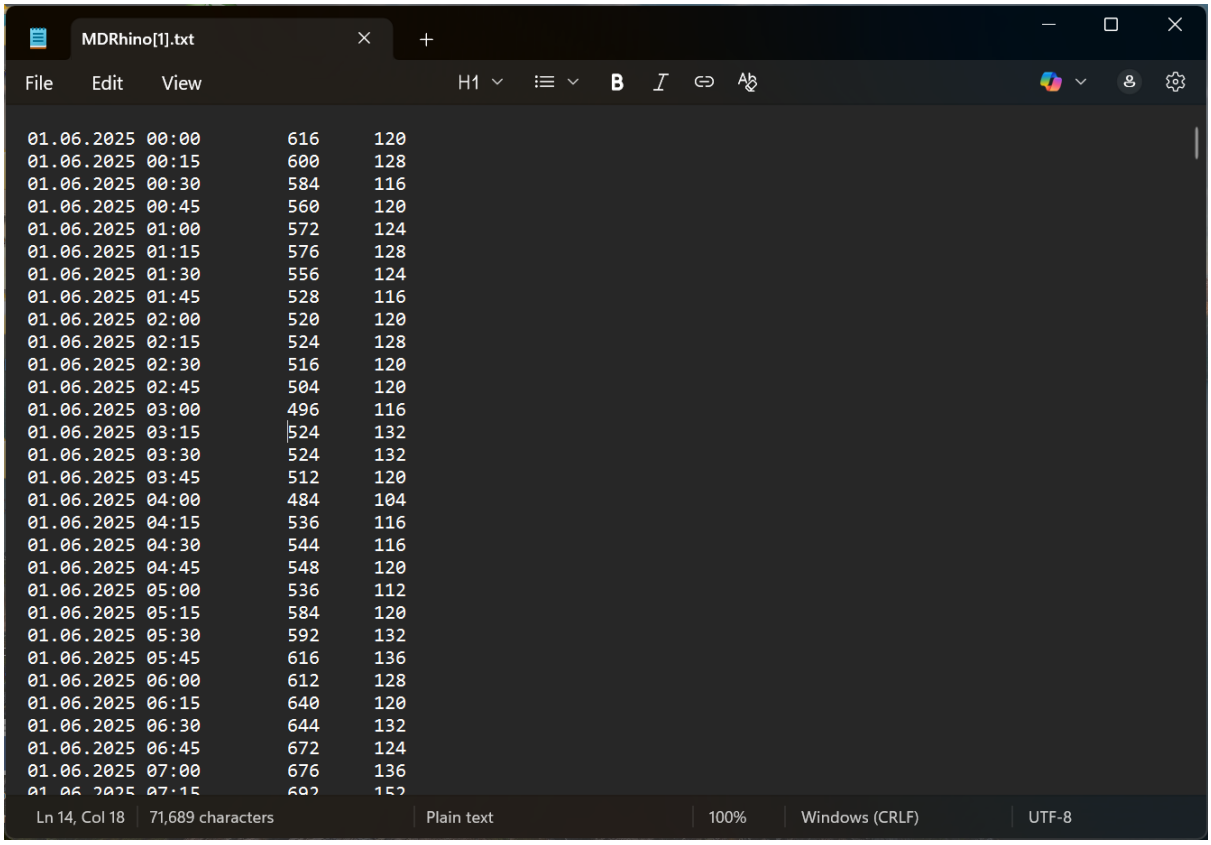

Figure 5: Sample feeder meter active and reactive power data used to input in the NEPLAN model for simulation analysis

A sample of the power demand characteristics during June 2025 in intervals of 15 minutes has been displayed in Figure 5 above, and it shows that there is a trend in the consumption of electrical energy in the distribution line. Figure 6 shows the power demand in a month in kVA, kW, and kVar. Moving closer, the daily 24-hour power demand for 01st June and 05th June 2025 in Figure 7 shows different consumption characteristics when considered individually.

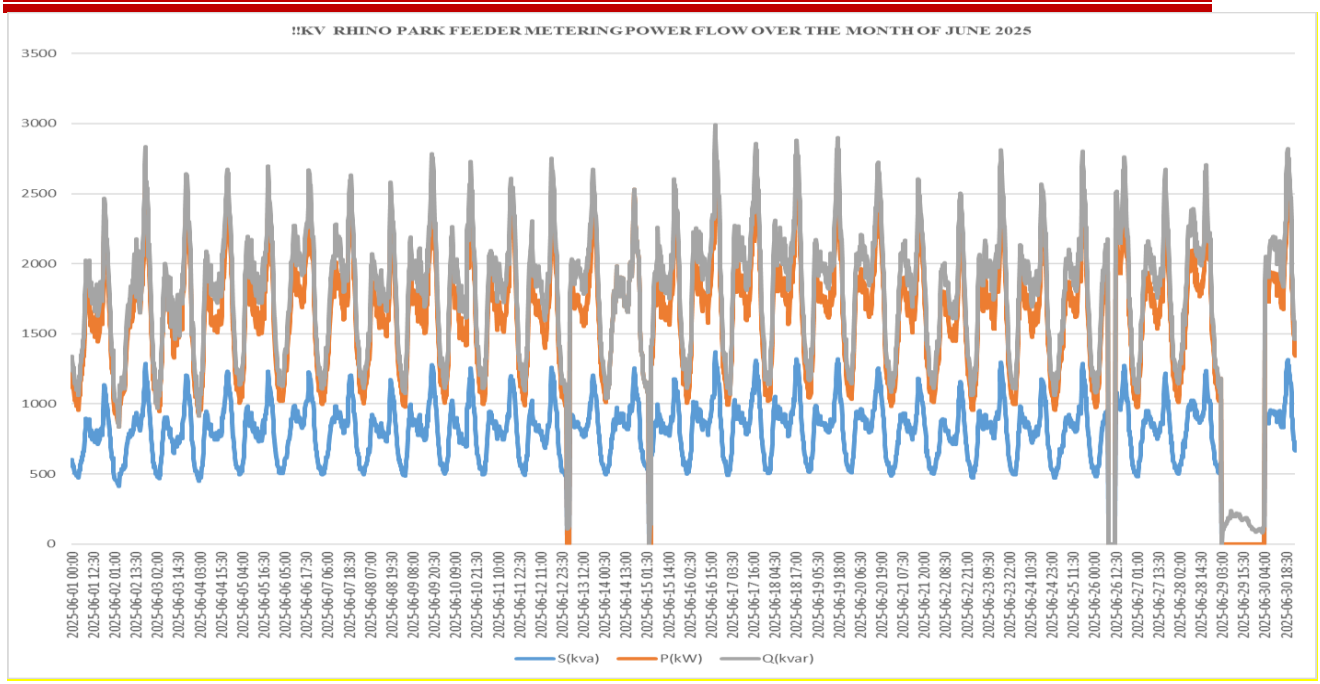

Figure 6: Power feeder measurement for the month of June 2025

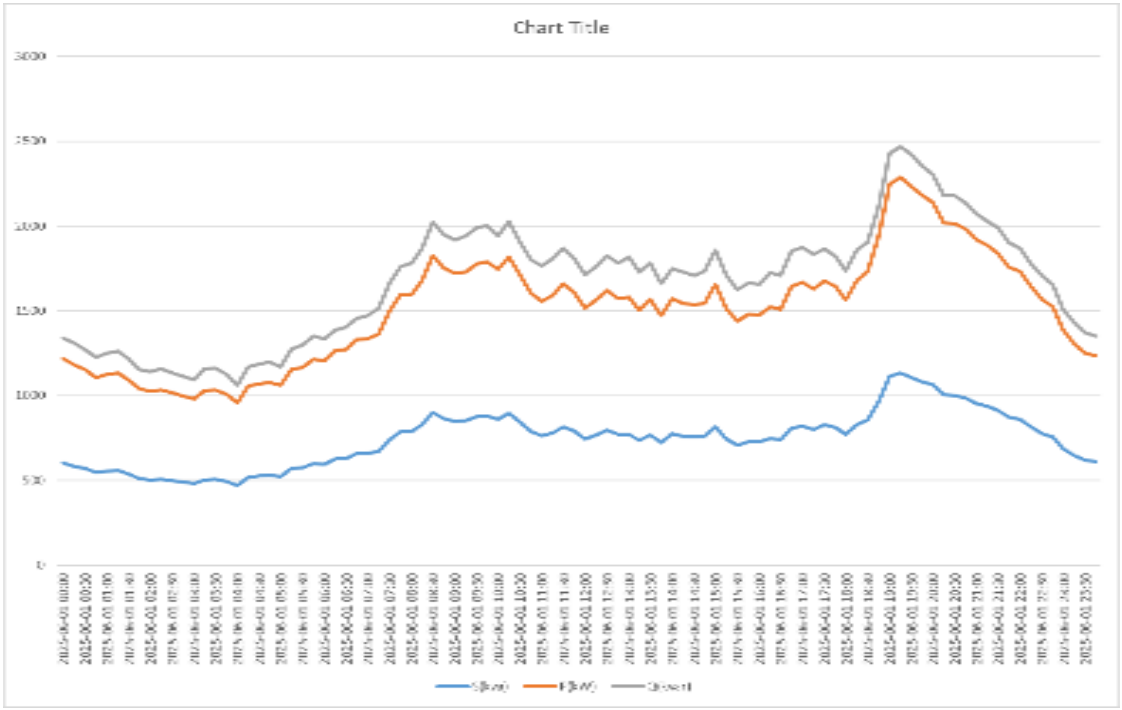

Figure 7: 24 hour Total, active and reactive power feeder measurement for 01st June 2025.

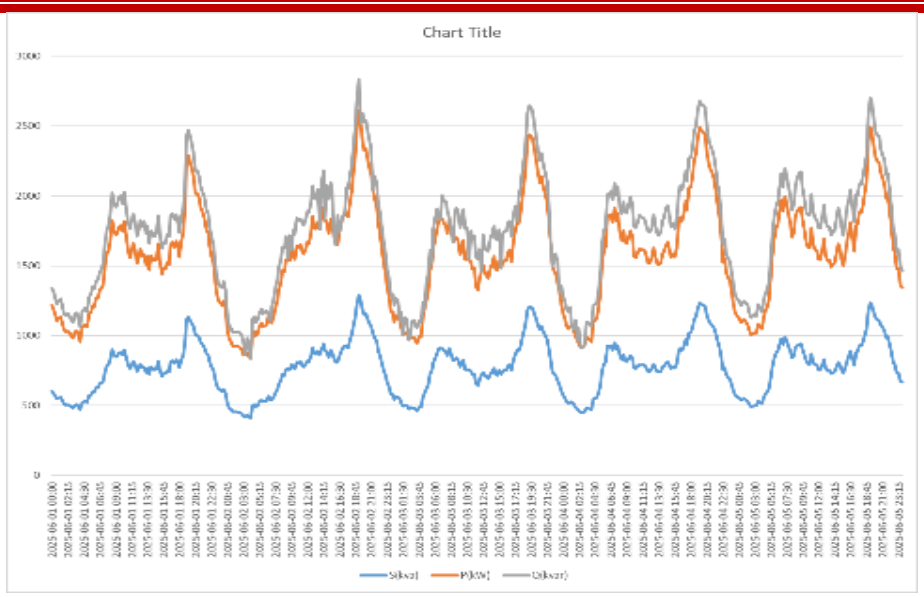

Figure 8: 24 hour Total, active and reactive power feeder measurement for 05th June 2025.

3.2. Results for loss reduction strategy optimization cost implication

The total cost function for evaluating the combined strategy is given by:

$$minC = C_{pl}^{i} + C_{rpc}^{i} + C_{dl}^{i} + C_{dt}^{i} \ldots\ldots$$

Where:

- C represents the total cost of the i-th loss reduction modification scheme;
- C_{pl}^{i} is the power loss cost;` Q
- C_{rpc}^{i} is the reactive power compensation cost;
- C_{dl}^{i} is the distribution line replacement cost;
- C_{dt}^{i} is the distribution transformer replacement cost.

From the above, the combined cost of replacement of the current existing system power lines and transformers will not provide the requisite benefits, even when we have seen that the change of conductor size results in a loss reduction. This is because the capital cost investment, coupled with the importation of the majority of power line hardware, attracts not only an import duty, but the cost of forex and installation. In addition, there will be a loss of sales due to outages to replace the existing equipment.

From table 8 and table 9 below, it has been demonstrated that the capital cost for change in the size of the conductor is exponentially greater (Ksh. 2,498,400) than the cost savings from the loss reduction cost (Ksh. 42,200). This therefore demonstrates that the 11kV distribution line was already optimized during its design.

Table 8: Power loss cost for the distribution feeder from exiting 75 mm^2 to 150mm^2 conductor size

Conductor size	Power loss (month of June2025) (MWh)	Electricity cost per unit (Ksh/kWh)	Total Units loss kWh	Total Cost (Ksh.)	Replacement cost from 75mm^2 to 150mm^2 (Ksh.)
75 mm^2	0.024	20	17,280	345,600	-
150 mm^2	0.021	20	15,120	302,400	43,200

Table 9: Replacement cost of conductor analysis for the distribution feeder from exiting 75 mm^2 to 150mm^2 conductor

Conductor size	Cost (Ksh./m)	Length (km)	Conductor Cost (Ksh.)	Labour and Transport Cost (Ksh.)	Replacement cost from 75mm^2 to 150mm^2 (Ksh.)
75 mm^2	64.50	12	2,322,000	-	-
150 mm^2	103.00	12	3,708,000	1,112,400	2,498,400

4. Discussion

From the results obtained for loss reduction strategies running separately for the power distribution network, the study has demonstrated a significant improvement in loss reduction across the 12km of 11kV network, down to the distribution transformers.

Specifically, the discussion on cost reduction and unit loss reduction will need to be examined separately, as constraints arise from the legal and regulatory compliance framework. The methodology used in this study aligns closely with that outlined in [2], which provided the basis for the strategies implemented here. The research focused on optimizing loss reduction in distribution networks, particularly through a comprehensive evaluation of power loss and cost-benefit ratios. [2] proposed an optimization model based on the replacement of distribution lines, upgrading of distribution transformers, and the incorporation of reactive power compensation. This approach is consistent with the loss reduction strategies explored in the current study, which considered similar aspects to improve network efficiency. The findings from this study support the methodology proposed by [2], as the power loss was significantly reduced across the distribution system, especially within the 12 km section of the network.

The results from both studies show that optimizing distribution networks through a combination of upgrading existing infrastructure can significantly reduce power losses. In [2], the optimization was done by balancing the cost-benefit ratio to determine the most cost-

effective strategy for loss reduction. Similarly, in this study, while specific cost implications were not fully explored due to regulatory constraints, the primary focus on loss reduction through similar optimization techniques indicates that the outcomes are in agreement.

Understandably, there have been some data gaps resulting from scheduled maintenance and controlled operations. However, the impact is not significant, as the one-month online data set was collected using a distribution feeder smart meter that has a communication link via a GSM network to the company's servers. It is important to note that some of the design considerations for the distribution network follow some of the geographical features of the terrain. In addition, wayleave acquisition or right of way plays a very key role, meaning that the design of the distribution network follows the county wayleave corridors, which usually means that the network is situated alongside the road network. This, therefore, means that there is a limit to the extent to which the loss reduction optimization strategy can be deployed.

5. Conclusions

Loss reduction optimization studies are very critical in the evaluation of distribution line design and development and its application fits well for both greenfield projects and existing networks. The loss reduction optimization application to existing networks may however face a few limitations and challenges, as retrofitting existing infrastructure to incorporate new optimization strategies and may involve some cost implications but, if well designed, the cost benefit analysis will depict it a worthwhile direction to take.

References

[1] S. Peyghami, P. Palensky and F. Blaabjerg, "An Overview on the Reliability of Modern Power Electronic Based Power Systems," IEEE Open Journal of Power Electronics, no. 1, pp. 34-50, 2020.

[2] J. Xie, C. Chen and H. Long, "A Loss Reduction Optimization Method for Distribution Network Based on Combined Power Loss Reduction Strategy," Complexity, vol. 2021, pp. 1-13, 2021.

[3] W. Strielkowski, L. Civín, E. Tarkhanova, M. Tvaronavičienė and Y. Petrenko, "Renewable Energy in the Sustainable Development of Electrical Power Sector: A Review," Energies, vol. 14, no. 24, pp. 1-124, 2021.

[4] E. H. Sadiq and R. K. Antar, "Minimizing Power Losses in Distribution Networks: A Comprehensive Review," Chinese Journal of Electrical Engineering, vol. 10, no. 4, pp. 20-36, 2024.

[5] D. Carr and M. Thomson, "Non-Technical Electricity Losses," Energies, vol. 15, no. 6, pp. 1-14, 2022.

Designing of a Control System for Automating Tank Farm Operations in an Oil Terminal during Oil Reception.

V. L. Mwalaa, D. W. Maina*

Kenyatta University, P.O. Box 43844-00100

* Corresponding author: dottymainaw@gmail.com

Abstract

A Terminal, is a platform used to store petroleum products it plays a strategic role in the oil and gas supply chain and ensures the success of an oil terminal business. A tank farm typically consist of multiple tanks or storage vessels that are interconnected and organized in a systematic manner in a terminal. Unfortunately most marine terminals in the country, are fully manually operated making operations quite strenuous particularly during the reception and stock taking stage. The reception stage is a critical operation in the logistics of petroleum products, this process begins with the mooring and berthing of the vessel at the wharf, followed by the methodical transfer of oil from the vessel's storage tanks to the terminal's bulk storage facilities. This transfer is accompanied by careful monitoring of flow rates, temperatures, and pressures to maintain quality and regulatory compliance making the entire operation labor intensive, it raises safety concerns and there is potential for human error. This begs the need for the integration of electronic sensors, Automatic Tank Gauging systems, and Supervisory Control and Data Acquisition technology to enhance efficiency, accuracy, and safety in managing storage and transfer processes. The automation framework designed and presented in this paper facilitates real-time monitoring of tank levels, flowrate, temperature, and pressure, enabling precise inventory management. This will overall improve operational reliability in the dynamic environment of oil reception and storage management. Such advancements signify improved operational reliability amid the evolving demands of oil reception and storage environments.

Key words: Terminal, Oil reception, Automated Gauging System (ATGs), Operational efficiency.

1. Introduction

Manual tank gauging has been used in the oil and gas industry for approximately 100 years. It entails using a dipstick which is a long, thin rod that was put all the way into the bottom of the tank. The ullage was then determined by reading the stick's marks and followed by the use of volumetric tank chart calibrations in order to determine the oil level in the tank, as the oil business expanded and tanks for storage grew in size, manual tank gauging became more

complex and time-consuming. One of the earliest known mechanical tank gauges was invented by Robert Peabody in 1885. Peabody's mechanical gauge utilized a float and pulley system to measure the level of liquid in storage. These devices used mechanical floats and pulleys to measure oil levels in tanks and display readings on a gauge.

The 1960s marked the initial adoption of electronic systems for ullage monitoring in oil and gas operations, revolutionizing inventory control and safety protocols. Early electronic gauging systems used basic electronic components and sensors to monitor liquid levels in storage tanks. The late 20th century and early 21st century saw widespread adoption of electronic gauging systems and software upgrades. Ultrasonic and radar-based sensors were introduced, allowing liquid levels to be measured without contact. Supervisory Control and Data Acquisition (SCADA) systems have also been integrated in tank gauging operations it enable real-time alerts, historical data analysis, and remote access capabilities, optimizing operational management and decision-making. These sensors with data processing units and control systems, enabling continuous monitoring of tank levels, temperature, and pressure. Most Modern tank gauging systems prioritize safety features such as leak detection, overfill protection, and automatic shut-off systems to mitigate risks and ensure regulatory compliance, most of the oil and gas ports and refineries now employ automated tank gauging systems and several significant corporations are creating their own systems. These systems contain Real-time data analytics to provide insights into operational efficiencies, inventory management, and resource allocation, supporting informed decision-making and cost savings.

2. Literature Review

This literature review explores current oil level detection methods, comparing traditional manual techniques with modern automated systems, and assess their impact on operational efficiency and safety. It will delve into the benefits and limitations of various oil level measurement technologies, evaluate the effectiveness of manual versus automated operations, and examine real-world case studies from leading companies to illustrate the practical implications of automation in tank farms.

2.1. Methods Being Used in Oil Level Detection in Tank Farms

Accurate detection of oil levels is essential for the effective management of tank farms, as it underpins operational efficiency, ensures safety, and facilitates compliance with regulatory standards. A range of measurement techniques is available, spanning from conventional manual methods to sophisticated sensor-based technologies.

2.1.1. Traditional Manual Methods and Semi- Automated Methods

Accurate oil level detection in tank farms is vital for operational efficiency, safety assurance, and regulatory compliance. Various techniques are used to measure oil levels, broadly categorized into manual, semi-automated, and fully automated methods. Traditional manual techniques, such as the use of dip tapes, dipsticks, thief gauges, and sight glasses, have long been utilized due to their low cost, simplicity, and minimal technological requirements. These methods involve the physical insertion of measuring devices into the tank to gauge oil levels. According to API Manual of Petroleum Measurement Standards (MPMS), manual gauging typically achieves an accuracy of ±3 mm for small tanks and up to ±1/8 inch with skilled handling. However, these methods are labor-intensive, prone to human error, and can pose safety hazards due to direct contact with hazardous substances and vapors (Instrumentation Tools, 2021)

To improve accuracy and minimize human involvement, semi-automated methods have been adopted in many tank farm operations. These include portable electronic gauges (PEGs) and closed gauging systems that can simultaneously measure ullage, temperature, and oil-water interface while maintaining sealed system integrity. PEGs improve repeatability and reduce emissions by operating through vapor-lock valves, thereby complying with environmental and safety regulations. Additionally, semi-automated methods enhance data accuracy and can store digital readings, which facilitates recordkeeping and trend analysis. Despite these improvements, these systems still require some operator interaction and regular calibration to ensure reliability (Universal Measurement & Control, n.d.; PDFCoffee, 2020). Overall, the transition from manual to semi-automated methods reflects an industry-wide shift toward enhancing accuracy, safety, and operational intelligence in fluid level measurement. These methods form the basis for more advanced automatic tank gauging systems, which integrate sensor technologies for continuous, remote monitoring and control.

2.1.2. Fully Automated Methods

Fully automated tank gauging (ATG) systems offer continuous, remote monitoring of liquid levels, interface detection, and environmental safety. These methods represent cutting-edge technology in oil level detection, offering high precision, reliability, and minimal human intervention. Ultrasonic level sensors use sound waves to detect the oil level, providing accurate measurements even in challenging conditions such as varying temperatures and pressures (Bailey & Wright, 2019). Guided wave radar (GWR) is another highly accurate automated method. It sends microwave pulses down a probe, which are reflected back when they hit the oil surface. GWR is known for its precision and reliability, making it ideal for

critical applications in tank farms (Chemical Processing, 2022). According to ISA, API MPMS Chapter 3.1B mandates that ATGs achieve level accuracy within ±3 mm compared to certified instruments, with overall inventory accuracy within ±25 mm, and feature tamper resistance and 1 mm resolution. These systems commonly employ guided-wave and non-contacting radar technologies, which boast immunity to vapor, foam, and fluctuating process conditions. Additionally, automatic gauges integrate temperature sensors and communicate readings to control centers, significantly reducing worker exposure risk and improving operational insights.

Figure 1: Shows a terminal operation.

2.1.3. Manual Gauging

Manual gauging involves the use of physical tools such as dipsticks and sight glasses. This method, while straightforward and cost-effective, is labor-intensive and prone to human error. In the context of oil storage tanks, the article highlights that manual gauging techniques, such as using dipsticks and sight glasses, are particularly prone to measurement inaccuracies. Systematic errors in manual gauging often result from calibration issues or inconsistencies in reading measurements. Chari (2012) notes that manual gauges may experience calibration drift over time, leading to incorrect readings, and emphasizes that human error, such as misreading scales or failing to adjust for temperature changes, further exacerbates inaccuracies. The study also addresses random errors that impact manual gauging, including environmental factors like temperature fluctuations that can alter the oil's volume and density. According to Chari (2012), these factors contribute to variability in manual measurements, as operators may not consistently account for them. The paper contrasts these manual methods with advanced measurement technologies such as radar and ultrasonic sensors, which provide greater precision and reliability. By offering real-time measurements and reducing the impact of environmental fluctuations, these modern technologies mitigate many of the limitations

associated with manual gauging (Chari, 2012). Thus, while manual tank gauging remains a common practice due to its simplicity and cost-effectiveness, the adoption of advanced technologies is recommended to improve measurement accuracy and operational efficiency.

2.1.4. Float-Based Sensors

Float-based sensors use the buoyancy principle to measure liquid levels. The float rises and falls with the oil level, and its position is detected by a sensor. This method is simple and cost-effective but can be affected by mechanical wear and fouling.

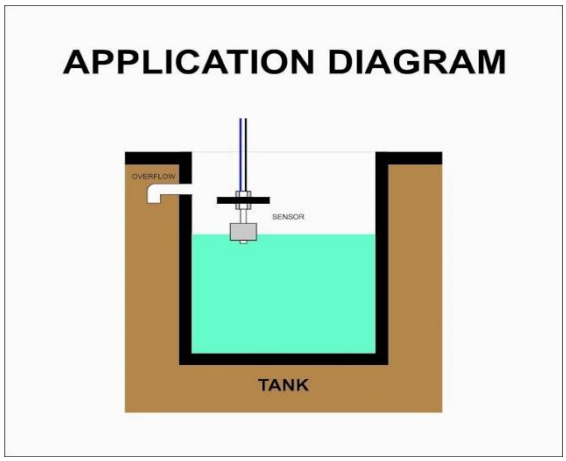

In their 2019 study, Kashyap et al. explored a novel approach for ultra-precision liquid level sensing using impedance spectroscopy and data analytics. This method provides higher accuracy and resolution compared to traditional float sensors, which can be limited by mechanical wear and environmental factors such as changes in liquid density or temperature. While float sensors rely on buoyancy and physical movement, the impedance-based technique measures changes in electrical properties, offering improved stability and reduced maintenance.

2.1.5. Radar and Ultrasonic Sensors

Radar sensors work by emitting microwave signals toward the surface of the oil, measuring the time it takes for the signals to reflect back to the sensor. Similarly, ultrasonic sensors use sound waves to achieve the same purpose. Both technologies are known for their high accuracy and reliability. Unlike float sensors, which rely on physical contact and buoyancy to detect liquid levels, radar and ultrasonic sensors measure the time-of-flight of their respective signals to determine the distance to the oil surface. This non-contact nature reduces the wear and tear associated with mechanical parts and minimizes the need for regular maintenance moreover, these sensors are less affected by environmental variables such as temperature and pressure changes.

2.1.6. Capacitive Sensors and Optical Sensors

Abass et al.'s study demonstrates that capacitive sensors provide reliable and consistent measurements of the oil-water interface, even under varying environmental conditions. This capability is particularly important for crude oil storage, where the presence of water can significantly impact the quality and processing of the stored oil. The automatic detection

system described in the paper eliminates the need for manual interface determination, which can be prone to human error and less accurate. The results from Abass's experiments show that capacitive sensing techniques can significantly improve the accuracy and reliability of interface measurements in crude oil tanks, making it a robust and efficient solution for modern tank farm operations. Abass concludes that the integration of capacitive sensing for interface determination in crude oil tanks represents a significant technological advancement, offering a practical solution to the challenges of liquid interface detection in storage environments (Abass, 2019).

Optical sensors use light to measure oil levels. They offer high precision and are suitable for detecting oil levels in clear liquids. Leal-Junior, Marques, Frizera, and Pontes (2018) explore the application of optical fiber sensors for multi-interface level detection in oil tanks in their paper published in Optical Fiber Technology. The study highlights the advantages of optical fiber sensors, which include high sensitivity, immunity to electromagnetic interference, and the ability to perform measurements in harsh environments. These sensors work by detecting changes in light transmission caused by variations in the refractive index at different liquid interfaces within the tank.

2.2. Comparison Between Automatic and Manual Tank Farm Operations

Manual tank farm operations depend heavily on human input for tasks like monitoring fluid levels, operating valves, and managing transfers. Tools such as mechanical gauges and float sensors are used, but these methods are labor-intensive and prone to error. As Abass et al. (2019) note, manual techniques often result in inaccurate readings due to inconsistent practices. In contrast, automated systems use technologies like SCADA and MPC to improve accuracy, safety, and efficiency. SCADA enables remote, real-time monitoring and control by integrating sensors that track levels, temperature, and pressure. This data helps operators make quick, informed decisions (Kashyap et al., 2019). Overall, automation significantly reduces human error, enhances efficiency, and optimizes resource use though it comes with higher upfront costs and cybersecurity concerns. While manual systems are cheaper and may suit smaller operations, automation is increasingly favored in larger, complex facilities.

2.3. Case studies around the world.

2.3.1. Case Study: Shell Oil

Shell Oil has integrated advanced radar and ultrasonic sensors into their tank farms to enhance measurement accuracy and reliability. Radar sensors use microwave signals to measure the distance to the oil surface, while ultrasonic sensors use sound waves for similar purposes. This

combination improves the precision of oil level measurements and reduces operational risks associated with inaccurate readings. “Radar Level Measurement in Oil and Gas Applications” by Vega Grieshabe discusses the application of radar technology in level measurement within the oil and gas industry. It covers the principles, benefits, and practical considerations of using radar sensors.

2.3.2. Case Study: British Petroleum (BP)

BP has employed automated control systems to streamline operations in their tank farms. These systems utilize real-time data analytics to monitor and control processes, thereby reducing manual labor and increasing operational efficiency. Automation helps in optimizing workflows, improving safety, and enhancing data accuracy. “The Future of Automation in Oil and Gas” by McKinsey & Company, discusses the future trends and impacts of automation in the oil and gas sector. It covers various technologies and strategies that are shaping the industry.

3. Methodology

This methodology outlines a comprehensive approach for designing a control system to automate tank farm operations during oil reception. The focus is on three primary objectives: measuring the inflowing oil level and temperature with high accuracy, and transmitting this data to a control room. The methodology includes detailed steps for each objective, ensuring thorough development and testing. When designing a control system, there are four key elements to take note of: Sensor Layer, Communication Layer, routed Network Layer and Application Layer.

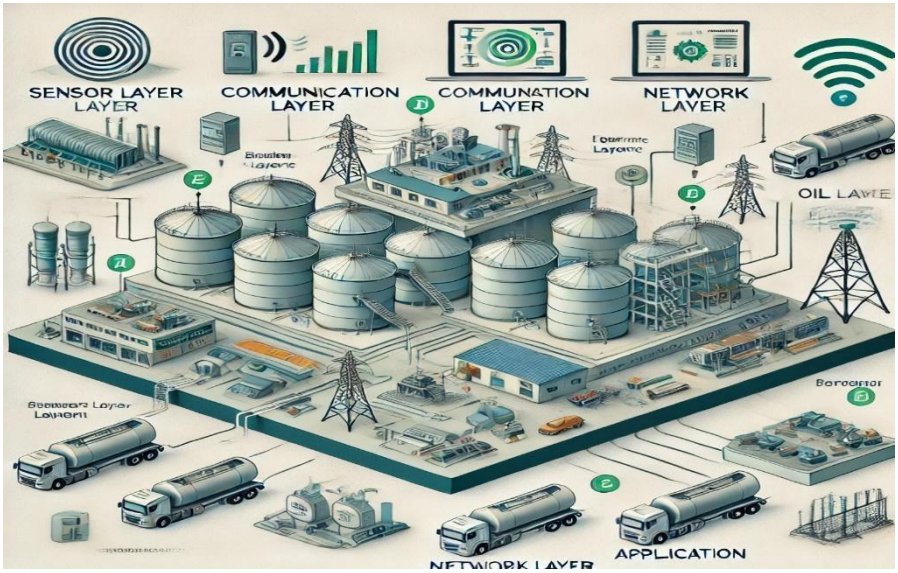

Figure 2. Shows four key elements in control system

Table 2: Key elements (Layers) of a control system

LAYER	DESCRIPTION
Sensor Layer:	This is the foundation of the system, where data collection happens. Sensors are used to measure key parameters like oil level, flow rate, temperature, and pressure in the tanks.
Communication Layer	This layer handles the transmission of data from the sensors to the control system. It ensures that the data collected by the sensors is accurately and reliably communicated to the central processing unit.
Network Layer	The network layer manages the routing and forwarding of data within the system. It ensures that the data from various sensors and control points is properly directed to where it is needed, whether it's to a local controller or a central server.
Application Layer	This is the top layer where the actual control and decision-making happen. It interprets the data collected from the sensors and uses it to automate the tank farm operations.

3.1.Measurement of Inflowing Oil Level

3.1.1. Sensor Selection and Specification:

The objective was to measure the level of inflowing oil in the storage tank with a margin of error of ±0.5 and determine the volume of the oil using an Ultrasonic Sensor. It measures distance by emitting high-frequency sound waves (ultrasonic waves) and calculating the time it takes for the echo to return after bouncing off the surface of the product. This method is effective for non-contact level measurement, which is ideal for various applications, including measuring the level of liquids like oil in tanks. These sensors consist of a transmitter that emits the ultrasonic pulses and a receiver that captures the reflected pulses. By measuring the time between the emission and reception of these pulses, the sensor can determine the distance to the product surface.

The distance measurement is calculated using the formula:

$$\textbf{Distance} = (\textbf{Time} \times \textbf{Speed of Sound}) / 2,$$

Where the speed of sound in air is approximately 343 meters per second at room temperature.

HC-SR04

The HC-SR04 is a widely used ultrasonic distance sensor known for its affordability and simplicity. It measures distance by emitting high-frequency sound waves from its transmitter and calculating the time it takes for these waves to reflect back to the receiver.

Figure 3. Shows a HC-SR04.

Reason for section:

- Affordability
- Ease of Use
- Non-contact Measurement
- Accuracy
- Wide Range: Capable of measuring from 2 cm to 400 cm, offering flexibility for various measurement needs.

Low Power Consumption: Operates efficiently with about 15 mA during measurement, making it suitable for battery-powered setups.

Compact Size: Small and lightweight, allowing for easy integration into various designs.

3.1.2. Setting up the ultrasonic sensor.

For setting up the ultrasonic sensor, it will be necessary to connect it to a microcontroller like the ESP32.

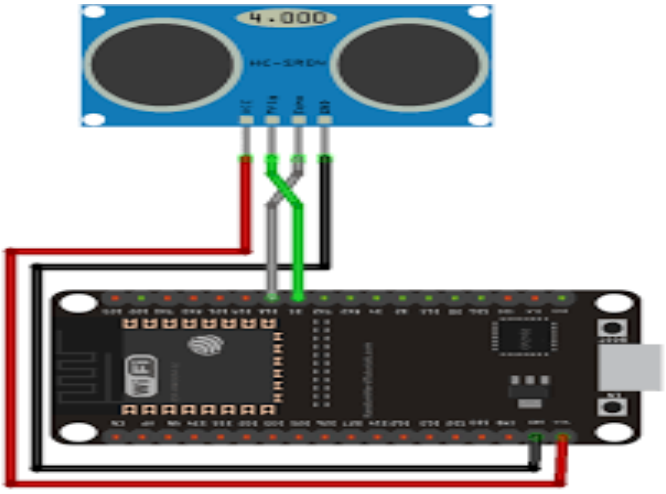

Figure 4. Shows an ultrasonic sensor.

The sensor, featuring four main pins—VCC (power supply), GND (ground), Trigger (initiates pulse emission), and Echo (receives the reflected pulse)—is connected as follows: VCC pin to the 5V output of the ESP32, GND pin to the ground pin of the ESP32, Trigger pin to a digital

output pin, and Echo pin to a digital input pin .Using jumper wires and a breadboard, these connections will be made to ensure stability and accuracy.

Programming the ESP32 involved coding it to control the ultrasonic sensor by sending a pulse from the Trigger pin, measuring the Echo response time, and calculating distance, which was displayed on the serial monitor. Calibration began by comparing sensor readings at a fixed height with known distances, adjusting code or sensor placement as needed. Field testing followed, with the sensor installed in a tank or test setup, and readings compared to manual measurements for accuracy. Calibration accounted for factors like temperature, surface reflection, and tank geometry.

3.2. Determining how to measure the product temperature in a storage tank using temperature sensors.

Temperature sensors, such as thermocouples or thermistors, are designed to provide accurate temperature readings by converting thermal energy into an electrical signal.

Infrared (IR) Sensors

Principle: Measure temperature by detecting the infrared radiation emitted by objects.

Features: Non-contact measurement

-Suitable for moving or hazardous objects

-Can measure surface temperature from a distance

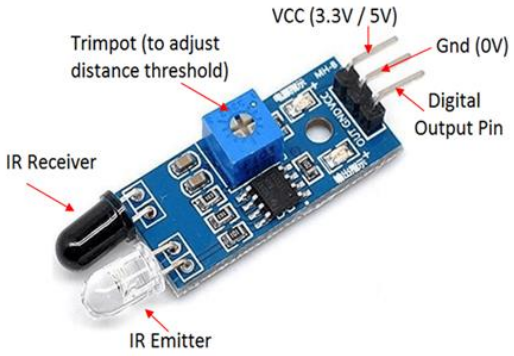

Figure 5. Shows an Infrared (IR) Sensors

In this project, the MLX90614 infrared temperature sensor with an ESP32 development board will be used to achieve precise non-contact temperature measurement.

3.2.1. Hardware Configuration

The initial step involved assembling the necessary components: the MLX90614 infrared sensor, ESP32 development board, a breadboard, and jumper wires. The MLX90614 is recognized for its capability to measure temperature by detecting infrared radiation emitted from objects, providing high accuracy without the need for direct contact.

Figure 6:

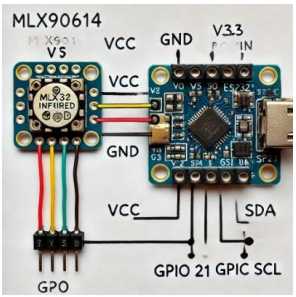

Figure 7

To set up the connections for the MLX90614 infrared temperature sensor with the ESP32, link the VCC pin of the MLX90614 sensor to the 5V pin on the ESP32 to provide the necessary power. Next, connect the GND pin of the sensor to the GND pin on the ESP32 to complete the circuit. For data communication, the SDA (data) pin of the MLX90614 should be connected to one of the ESP32's GPIO pins, while the SCL (clock) pin of the sensor is connected to another GPIO pin.This setup facilitates communication between the sensor and the ESP32 through the I2C protocol, allowing for data transfer and temperature readings.

3.3. Determining how to transfer (send and receive) instructions and the sensors data wirelessly from storage tank to a web dashboard in a tank farm control room.

To facilitate the wireless transfer of sensor data and instructions from a storage tank to a web dashboard located in a tank farm control room, we implemented a comprehensive Wi-Fi-based communication system.

Data Acquisition

Temperature sensors (MLX90614) are installed in storage tanks to measure oil temperature without contact. Each sensor connects to an ESP32 board, which reads the temperature data at intervals, formats it into JSON, and prepares it for network transmission.

Wireless Transmission

The ESP32 uses Wi-Fi to send data via HTTP to a web server on the tank farm's network. Transmission is optimized for low latency and real-time updates.

Web Dashboard Integration

A React.js-based dashboard displays temperature data using real-time charts (Chart.js). WebSocket connections ensure instant updates, providing users with live readings, trends, and alerts.

4. Results & Discussion

Figure 8. Actual prototype set up.

4.1. Determination of the product level in tanks as a fulfilment of the first objective

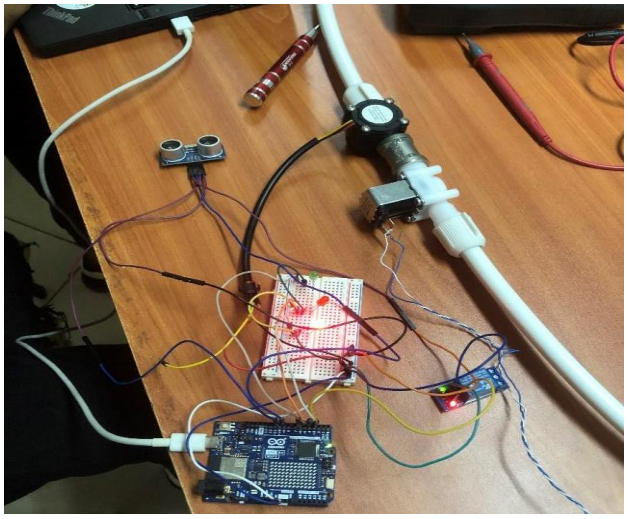

Figure 9: Hardware setup

Figure 9 shows a hardware setup involving an Arduino board, a breadboard with LEDs, a relay module, a flow meter, and a solenoid valve.

Key Components:

1. Arduino Board (Bottom Left):
   - Acts as the central controller, receiving sensor inputs and controlling outputs.
   - It is connected to a computer for programming and monitoring.
2. Ultrasonic Sensor (Top Left):
   - Used for measuring distance or level, possibly to detect fluid levels or monitor a tank.

3. Breadboard (Center):
   - Contains LEDs for visual feedback, likely indicating system status or operation.
   - Wired connections link components to the Arduino.
4. Relay Module (Bottom Right):
   - Used to control high-power devices (like the solenoid valve) from the Arduino.
5. Solenoid Valve (On Pipe):
   - Mechanically regulates the flow of liquid through the pipe.
   - Controlled by the relay module.
6. Flow Meter (Connected to Pipe):
   - Measures the rate of fluid flow through the system.
   - Sends data to the Arduino for processing.

This system uses the Arduino IDE to write and upload code to an ESP32 development board, which acts as the controller for the program. The ultrasonic sensor in the setup measures the distance from the top of the tank to the surface of the petroleum product. Using this measured distance and the known height of the tank, the system calculates the actual level of the petroleum product inside the tank.

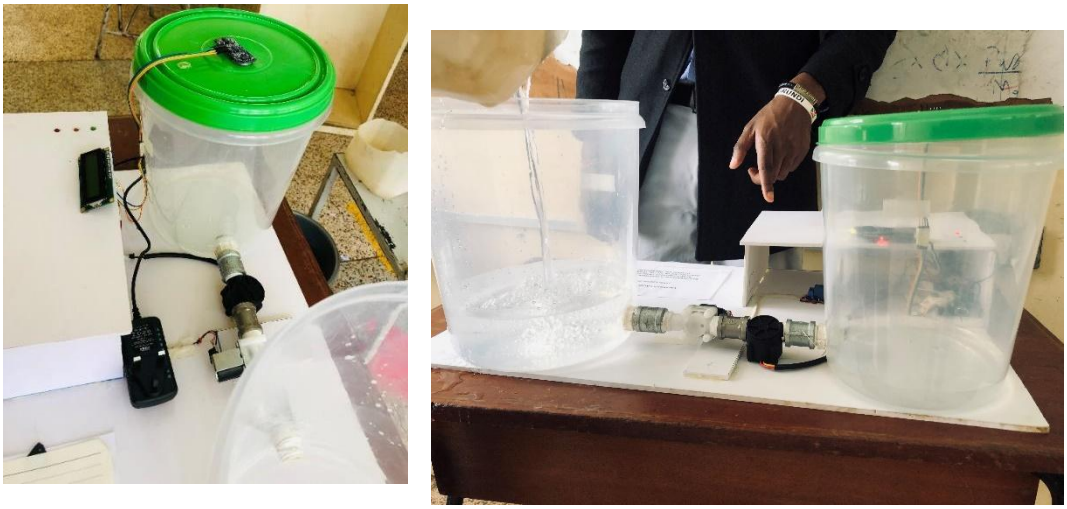

Figure 10. Shows components for this objective's operation.

The code for the system was successfully compiled and uploaded to the ESP32 via a USB connection. To test the system, a tank with a height of 30cm was filled with petroleum product. The level readings were then continuously monitored and recorded in real time through the serial monitor of the Arduino IDE. These readings were observed over a period to validate the system's performance on LCD.

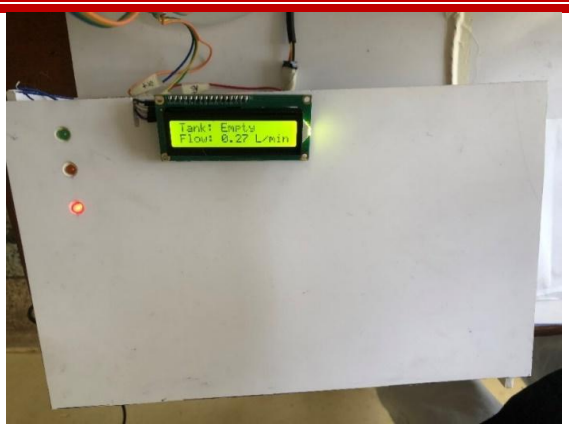

Figure 11.Shows an LCD operation.

4.2. Determination of the product temperature in tanks as a fulfilment of the second objective

It utilized a temperature sensor integrated with an Arduino-based system to measure and monitor the temperature of the product in storage tanks. The Arduino IDE was used to write and upload the program to the ESP32 development board, which acted as the main controller. A temperature sensor was connected to the ESP32, enabling it to measure the temperature of the product inside the tank accurately. The collected data was processed in real time and displayed on the serial monitor of the Arduino IDE for observation and analysis.

During the testing phase, the system demonstrated its ability to capture precise temperature readings from the tank, validating the accuracy of the setup.

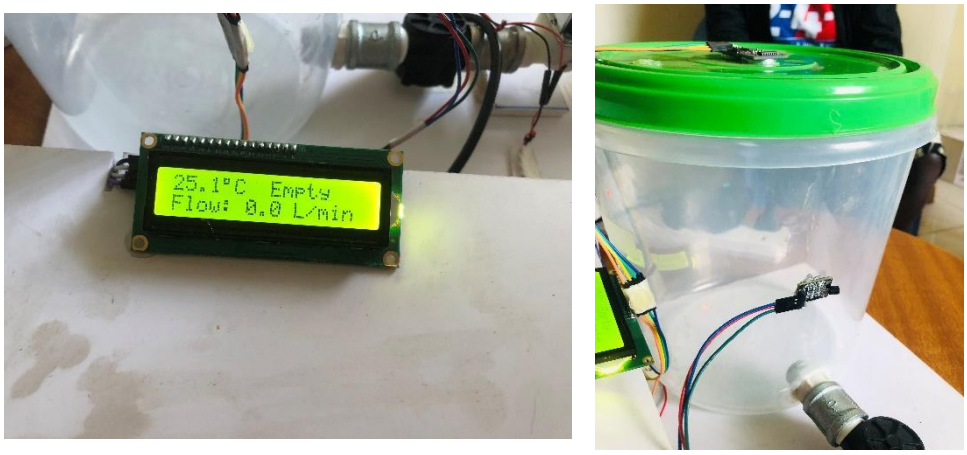

Figure 12. Shows the temperature display operation.

During the testing phase, the system was able to provide real-time temperature-related results, demonstrating the effectiveness of combining ultrasonic sensing technology with an Arduino-based control system for industrial applications. The results were recorded systematically to validate the accuracy and reliability of the setup.

4.3. Transfer (send and receive) instructions and the sensors data wirelessly from storage tank to a web dashboard as a fulfilment of the third objective.

The dashboard provides a graphical representation of the data, which allows a user to monitor the product level and temperature in the tank remotely. The dashboard provided real- time updates of the data, which allowed the user to take appropriate action if the product level or temperature went out of the set limits.

The use of IoT technology eliminates the need for manual monitoring, which can be time-consuming and prone to errors.

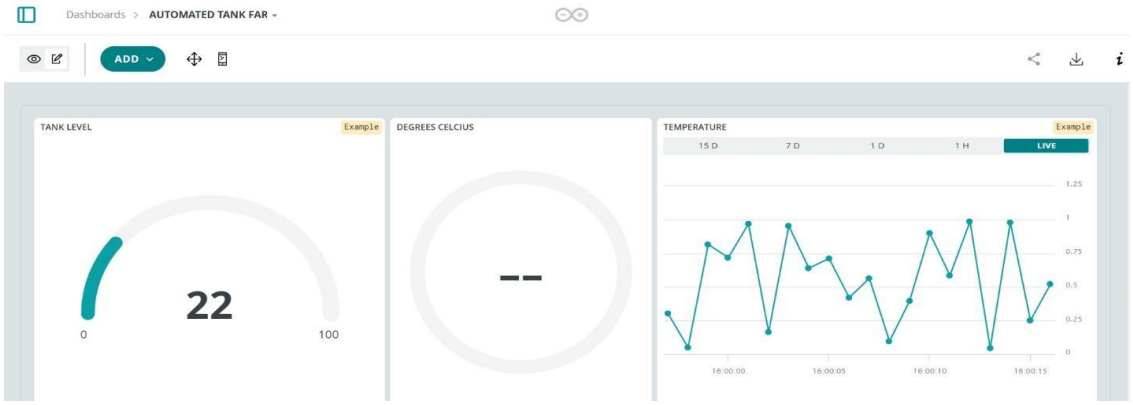

Figure 13. Cayenne Dashboard showing real time product level, temperature, product temperature chart and Tank utilization Chart

5. Conclusion

The liquid level in the tank was accurately assessed using an ultrasonic sensor system, which operates by emitting sound waves and capturing the echoes reflected from the liquid surface. The measured values were displayed in real time on the serial monitor of the Arduino IDE, enabling immediate visualization of tank levels. Additionally, the temperature of the liquid was successfully measured using a contactless infrared temperature sensor, with the data similarly presented on the Arduino IDE's serial interface for continuous tracking of temperature variations. Both the liquid level and temperature readings were then transmitted wirelessly to an online dashboard, facilitating real-time and remote monitoring of tank conditions through a web-based interface.

6. Recommendations

It is recommended to adopt radar-based level sensing technologies in place of ultrasonic sensors to enhance measurement accuracy, extend operational range, and improve reliability in challenging environmental conditions. Radar sensors offer superior performance in scenarios where ultrasonic signals may be compromised by factors such as dust, vapor, or

foam, thereby ensuring more consistent and precise liquid level detection in tank monitoring applications.

References.

1) Abass, A. M. M., Sestok, C. K., Dabak, A. G., Ramaswamy, S., & Kumar, R. (2019). Automatic determination of liquid's interface in crude oil tank using capacitive sensing techniques. Journal of Engineering, 25(12), 114–121.
2) American Petroleum Institute. (2013). Manual of petroleum measurement standards, Chapter 3.1A: Standard practice for the manual gauging of petroleum and petroleum products (3rd ed.). Washington, DC: Author.
3) American Petroleum Institute. (2021). Manual of petroleum measurement standards, Chapter 3.2: Electronic gauging systems (4th ed.). Washington, DC: Author.
4) Automation.com. (2017). Improving worker safety with automatic tank gauging. Automation.com.
5) Bailey, D., & Wright, E. (2019). Practical SCADA for industry. Elsevier.
6) Chari, S. R. (2012). Storage tank–measurement errors and accuracy. Indian Journal of Fertilisers.
7) Chkara, K., & Seghiouer, H. (2020). Criteria to implement a supervision system in the petroleum industry: A case study in a terminal storage facility. Advances in Science, Technology and Engineering Systems Journal, 5(5), 29–38.
8) Dhanraj, J. A., Krishnamurthy, B., Ramanathan, K. C., Saravanan, A. K., & Raman, J. K. G. (2020, December). Design on IoT-based real-time transformer performance monitoring system for enhancing the safety measures. In IOP Conference Series: Materials Science and Engineering (Vol. 988, No. 1, p. 012076). IOP Publishing.
9) Instrumentation Tools. (2021). Manual level measurement methods. Instrumentation Tools.
10) International Society of Automation. (2018). Guided-wave radar for inventory tank gauging. InTech, July–August.
11) Kashyap, B., Sestok, C. K., Dabak, A. G., Ramaswamy, S., & Kumar, R. (2019). Ultra-precision liquid level sensing using impedance spectroscopy and data analytics. IEEE Sensors Journal, 19(20), 9468–9478.
12) Kolvekar, K., Lotlikar, S., Naik, M., Faldesai, A., Muttu, Y., & Colaco, M. (2020, December). Cayenne-based plant monitoring control system. In 2020 IEEE Bombay Section Signature Conference (IBSSC) (pp. 237–242). IEEE.

13) Leal-Junior, A. G., Marques, C., Frizera, A., & Pontes, M. J. (2018). Multi-interface level in oil tanks and applications of optical fiber sensors. Optical Fiber Technology, 40, 82–92.

14) Marques, R., de Paula Ferreira, W., Nassif, G., Armellini, F., Dungen, J., & de Santa-Eulalia, L. A. (2021). Exploring the application of IoT in the service station business. IFAC-PapersOnLine, 54(1), 402–407.

15) Universal Measurement & Control. (n.d.). Manual gauging and sampling systems. Universal Measurement & Control.

INSTRUCTIONS TO CONTRIBUTORS

The editorial staff of the AJERI requests contributors of articles for publication to observe the following editorial policy and guidelines accessible at https://www.iekenya.org/ in order to improve communication and to facilitate the editorial process.

Criteria for Article Selection

Priority in the selection of articles for publication is that the articles:

a. Are written in the English language

b. Are relevant to the application relevant of engineering and technology research and Innovation

c. Have not been previously published elsewhere, or, if previously published are supported by a copyright permission

d. Deals with theoretical, practical and adoptable innovations applicable to engineering and technology

e. Have a 150 to 250 words abstract, preceding the main body of the article

f. The abstract should be followed by a list of 4 to 8 "key Words"

g. Manuscript should be single-spaced under 4,000 words (approximately equivalent to 5-6 pages of A4-size paper)

h. Are supported by authentic sources, references or bibliography

Rejected/Accepted Articles

a. As a rule, articles that are not chosen for AJERI publication are not returned unless writer (s) asks for their return and are covered with adequate postage stamps. At the earliest time possible, the writer (s) is advised whether the article is rejected or accepted.

b. When an article is accepted and requires revision/modification, the details will be indicated in the return reply from the AJERI Editor, in which case such revision/modification must be completed and returned to AJERI within three months from the date of receipt from the Editorial Staff.

c. Complementary copies: Following the publishing, three successive issues are sent to the author(s)

Procedure for Submission

a. Articles for publication must be sent to AJERI on the following address:

The Editor

African Journal of Engineering Research and Innovation

P.O Box 41346- 00100

City Square Nairobi Kenya

Tel: +254 (20) 2729326, 0721 729363, (020) 2716922

E-mail: editor@iekenya.org

b. The article must bear the writer (s) name, title/designation, office/organization, nationality and complete mailing address. In addition, contributors with e-mail addresses are requested to forward the same to the Editor for faster communication.

For any queries, authors are requested to contact by mail (editor@iekenya.org).

PUBLISHER

The Institution of Engineers of Kenya (IEK)

P.O Box 41346- 00100

City Square Nairobi Kenya

Tel: +254 (20) 2729326, 0721 729363, (020) 2716922

Email: editor@iekenya.org

Website: www.iekenya.org

CONTENTS **Pages**